1 Abstract

Ignition systems have fundamentally remained unchanged since the dawn of the internal combustion engine industry. In order to respond to new legislation, the necessary improvement on fuel economy and lowering emissions, new technologies are being considered to attain increasingly strict parameters.

One of such technologies is the use of a corona discharge ignition system. Corona discharge or partial discharge is a phenomenon where high voltage combined with high frequency and high spatial gradient creates an ionic plasma region around the electrode with high ionizing effect on the surrounding medium.

This phenomenon has been recorded and studied in the past, but has only recently been proposed as an ignition source, with several interesting advantages over century-old sparkplug arc ignition technology.

The matter of this thesis is to analyze the physics of the phenomenon, to construct a device capable of performing measurements on the phenomenon, and ultimately to test if such an ignition device is possible and useful in the industry.

Furthermore, any results determined by this thesis will be able to set a starting point for further research on the matter.

2 Table of contents

3 Introduction

The motivation for this study came from taking an interest in the performance of flame holding devices in gas turbines under highly stressing conditions. This was a subject which was very difficult to develop experiments for in a lab, and there was a distinct interest from the beginning that for this study for there to be a significant amount of experimental data to acquire.

After investigating the state of the art of corona discharge ignition technology we realized that the applications to flux heat engines were still unclear. However, some promising leads were found, which are detailed further on in this memoir.

The main objective of this work was to produce a device capable of probing the phenomenon of corona discharge in order to measure its parameters, and to experimentally test its ignition technology potential.

After the measuring methodology was designed, the required equipment was obtained through construction or was readily available in the lab. The construction of the measuring equipment was to be an important factor in the study.

The measures would provide data for analysis to fully understand the phenomenon and to theorize about, and if possible demonstrate, the possible use as an ignition device.

Finally, all unresolved matters will be identified and compiled to provide starting points for future research studies.

4 State of the art

4.1 Technology overview

The technology used today for the ignition of heat engines has remained fundamentally unchanged since the first modern internal combustion engine was built in 1860. The engine, built by Belgian engineer Jean Joseph Etienne Lenoir, used a Rhumkorff coil, with a switch to interrupt the current to an inductor, to produce a voltage surge (About.com). The voltage surge suffices to cause dielectric (air and fuel mixture) breakdown, and thus, a spark.

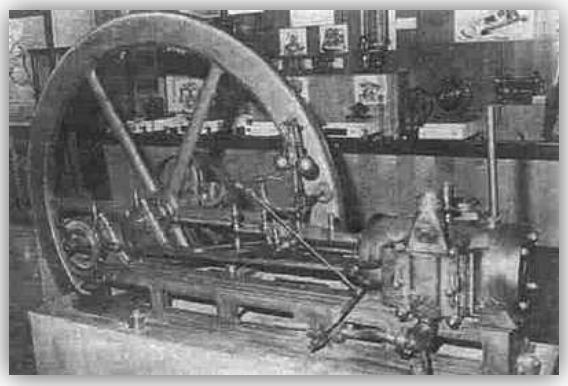

Fig. 1 The Lenoir motor. Musée des arts.

Over time, spark plugs have evolved, mainly shaped by new technologies that affect engines globally. In the past decade engines have consistently grown smaller. This is because overall smaller engines have better efficiencies than large engines; and consequently spark plugs have been made smaller. Smaller engines tend to have randomly abnormal combustion, so spark plugs may be under heavy mechanical and thermal stress, aside from already requiring, for example, high dielectric strengths. However, they have fundamentally remained unchanged. (Hargreaves, 2013)

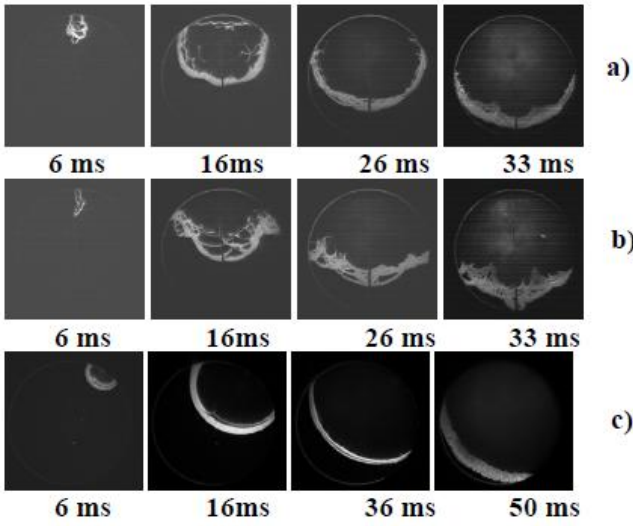

Fig. 2 a) and b) show flame boundaries of corona ignited mixtures, while c) shows a sparkplug ignited one. Note the time frame reduction (Bellenoue, 2005).

Spark igniters present a series of problems which may be addressed with new technologies. Sparks cause a one-point ignition, so the flame must advance at natural speed. This speed is sufficient but the benefits of burning a greater volume simultaneously are not negligible. This must be done by igniting the mixture all at once, i.e. a volume ignition instead of a single point ignition. In several experiments high fuel burn speeds have demonstrated higher pressure increases as well as lower heat losses, which could produce significant efficiency improvements.

The spark ignition sequence can be divided into four phases:

1- Pre-breakdown. The voltage surge is applied and electrons are accelerated towards the anode. This ionizes the gap and diminishes the impedance of the medium until breakdown is achieved, typically in under 1ns. The energy transfer between electrodes does not trigger ignition in this phase.
2- Breakdown. Energy is deposited in the volume enclosed by a 50µm cylinder in the spark plug gap. Temperature of the plasma at the tip of the electrode rises to 60,000K, which causes a supersonic expansion. The current flow (~100A) is permitted by a drop in the gap's impedance.
3- Arc. Low current flow (>0.1A) at low voltage (~100V). More energy is transferred during this phase than during breakdown, but at a lower power than during the breakdown phase. Temperature of the plasma is now ~6,000K.
4- Glow. Only currents under 100mA are sustained for a time in the millisecond range. In this phase there are high heat losses and low energy transfer (Dale, Checkel, Smy, 1997).

Spark ignition presents many issues and several alternatives have been proposed and investigated; one being corona discharge ignition. Much research has been done on corona

discharge ignition devices. However throughout the ‘90 there have been several leads directed to innovate on ignition devices in general. The alternatives to conventional spark plugs being:

- Laser ignition.
- Microwave ignition
- High-frequency plasma stream

Using a laser, ignition initiates in a line instead of a point and can remain on as a continuous ignition source. By using mirrors, there may be several beams which can produce ignition. This can indeed enhance the burning rate by creating several lines of ignition. However there are many problems using optical systems in combustion chambers, aside from the size of a device capable of transferring enough energy into the combustion chamber.

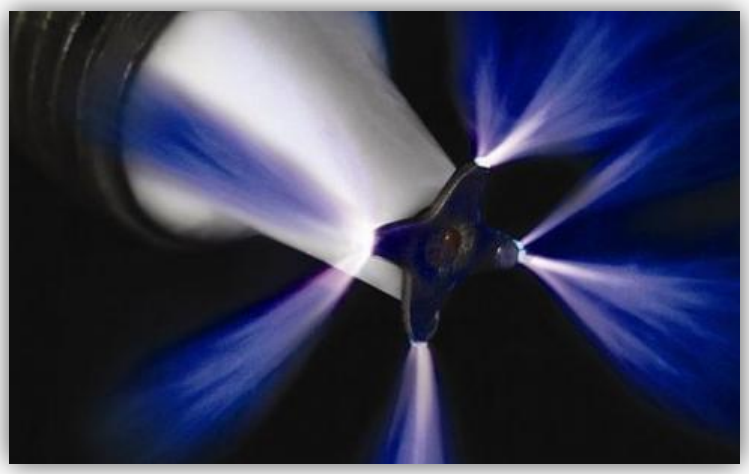

Fig. 3 still of the electrode of Federal-Mogul’s Advanced Corona Ignition System (ACIS) while discharging. Probably a rendered image.

Microwave ignition presents very interesting results in theory; however experiments have shown it to ignite in one single point as well, at 2.45GHz. To attain volume ignition, frequencies must be between 80 and 100 GHz which require a very large device to be generated. This makes it impractical to mount in a conventional vehicle. (Hargreaves, 2013)

High frequency plasma stream produced by a corona effect electrode presents several advantages in both ionization section (i.e. volume of ignition) and device simplicity. Additionally, the required energy transferred to the fluid for ignition is transferred more efficiently as it is distributed throughout a much larger volume than an arc spark. This effectively reduces energy consumption and speeds up the combustion, which leads to higher-pressure increase and smaller thermal losses.

The following graphs surmise the key factor of improvement in corona discharge ignition devices versus traditional spark ignition devices.

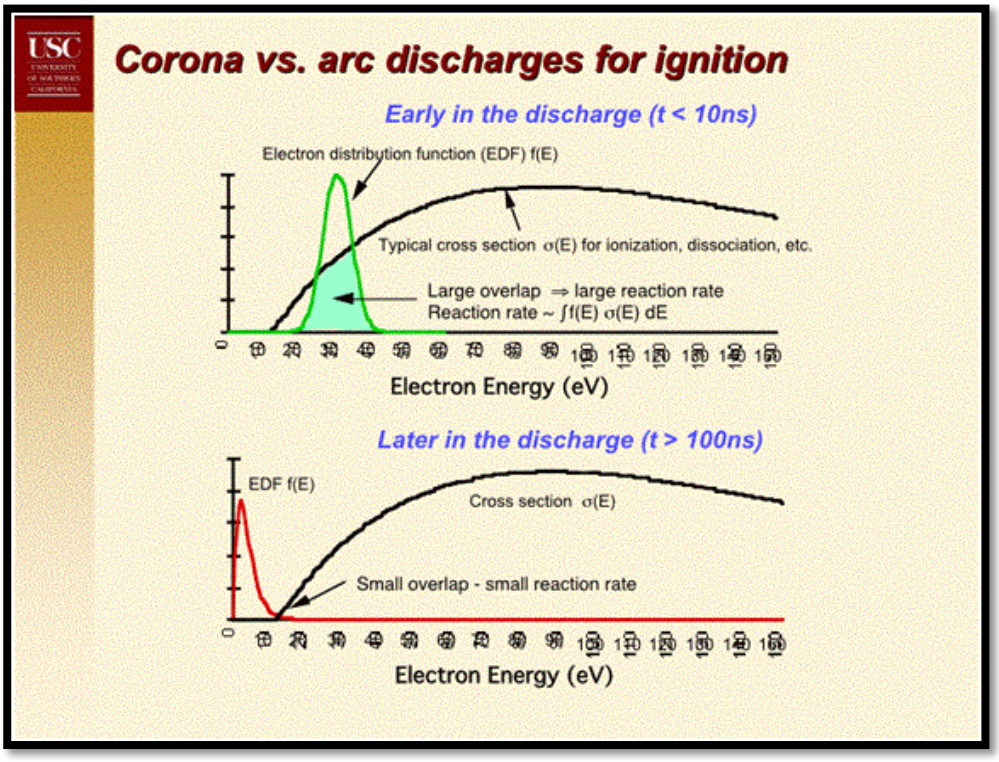

Fig. 4 (Ronney, 2004).

In Figure 4, there are two probability graphs corresponding to corona discharge ignition and spark ignition at the time ignition starts. In both, the mixture and geometric properties of the setting are identical, i.e. the mixture has the same ratio, is at the same pressure and the chamber geometry is identical, excluding, of course, the electrode. In both cases the probability function for ionization of the medium is thus equal, represented by a black solid line.

The first graph is a still of the electron's distribution function against its energy taken during the corona discharge (t<10ns). The electron distribution function presents a relatively high and narrow energy distribution, largely overlapping the cross section for ionization. Since the arc is never achieved, electrons ionizing the electrode's surrounding medium have very high energy in a significantly large section (volume) compared to the reduced volume directly in contact with a spark (Ronney, 2004). This results in a very efficient energy transfer from the electrode into the medium. The probability of high energy electrons (throughout the whole energy spectrum) overlapping with a large volume of mixture is very high.

In contrast, in the second graph (t>100ns) the probability for the medium to become ionized is overlapped only by a minute part of the electron distribution function generated by the spark. This is mainly due to the spark having a small area of influence. In fact, a spark can be modeled as a cylinder measuring 50µm in diameter between anode and cathode in the sparkplug, resulting in a volume between .002 and .003 mm^3 (Dale, Checkel, Smy, 1997).

4.2 Corona discharge

Also known as a partial discharge, it is an electrical energy emission caused by ionizing a conductor's surrounding fluid by attaining a certain value in the electrical field's potential gradient. When the electrical field's potential gradient reaches this value, the medium becomes ionized and thus conductive. As frequency increases, the minimum potential gradient for corona discharge to occur decreases.

It is likely that this phenomenon was first identified as fires or torches in the masts of sailing ships during thunderstorms, and was thought to have divine origins. These fires were in fact plumes of ionic plasma emanating from the tips of ships mast because of the electric field's potential gradient buildup, caused by electrically charged clouds.

It is interesting how this phenomenon has been observed since ancient times; the first written mention of it being in the Castor and Pollux myth poem written by Alcaeus of Mytilene[1], or the 33rd Homeric Hymn to Castor and Pollux, also named the Dioscuri[2], both written between the 7th and the 6th century BC.

[1] Come to me, from Pelops' isle departing, / brave and steadfast children of Zeus and Leda; / show yourselves with generous, kindly spirits, / Castor and Pollux, // who across the broad and expansive earth and / all the sea on swift-footed horses fly and / rescue humans easily from the frigid / coldness of dying,/ vaulting up the heights of the well-benched ship's masts / glowing far, ascending the forestays in the / dismal nighttime, bearing the blazing fire for / shadowy vessels.

[2] Bright-eyed Muses, tell of the Tyndaridae, the Sons of Zeus, glorious children of neat-ankled Leda, Castor the tamer of horses, and blameless Polydeuces. […] but the strong wind and the waves of the sea lay the ship under water, until suddenly these two are seen darting through the air on tawny wings. […].

Many other accounts of the naturally occurring corona discharge phenomenon have been variedly named throughout history, mainly by sea-faring cultures.

Electrode shapes are fundamentally important both for augmenting the potential gradient and to determine the total volume of ionized medium, as streamers will emanate from each geometric region with low surface curvature radius, i.e. sharp.

Fig. 5 Undesired occurrence of corona discharge in high voltage power lines, causing power losses. Objects with large curvature radius are less likely to produce corona discharge when a high electric potential is applied, due to them creating weaker gradients. This image has an exposure time of 92 seconds, so the corona discharge flares are actually very weak, and thus invisible to the naked eye. Image credit: *Nitromethane* Wikimedia user.

Energy losses in power lines are still mainly due to resistive losses from electrical current. By increasing the voltage of power transmission lines, the current can be decreased, reducing resistive losses by a squared factor. However in high voltage power lines (over 2.000kV) the corona discharge losses can surpass the resistive losses.

Corona discharge occurs in phases as follows:

1. A neutral particle is spontaneously ionized by a natural environment event and an electron becomes separated.

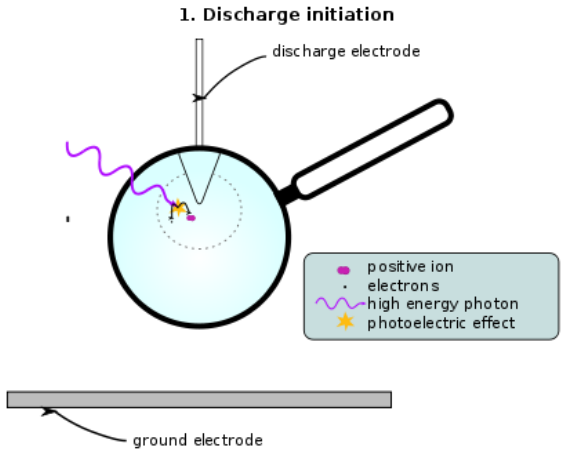

Fig. 6 (Public domain).

2. The electric field created by the electrode separates these particles in opposite directions, imparting kinetic energy to both of them.

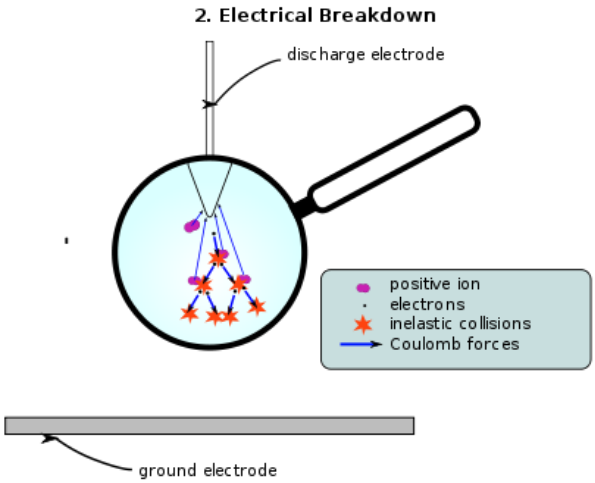

Fig. 7 (Public domain).

3. The electron is accelerated to a higher velocity by having a much larger charge-to-mass ratio than the positive ion. Such is this speed that on impacting another particle, it becomes ionized by it releasing another electron. Increasingly, electrons are separated from atoms in the electric field, causing what is known as an electron avalanche.

4. As the electrons collide with positive ions, they recombine to form neutral particles. When this happens, the electron falls back to its original energy level releasing a photon of light. The electron avalanche does not release enough energy to heat the gas, as opposed to a spark, so the ionized medium creates a region of non-thermal plasma around the electrode. If the medium surrounding the electrode had a mixture of fuel and air, ignition through ionization could occur. The fuel particles would in fact be irradiated by high energy photons (not heated), which transmit the activation energy required by the fuel to become oxidized by nearby oxygen molecules.

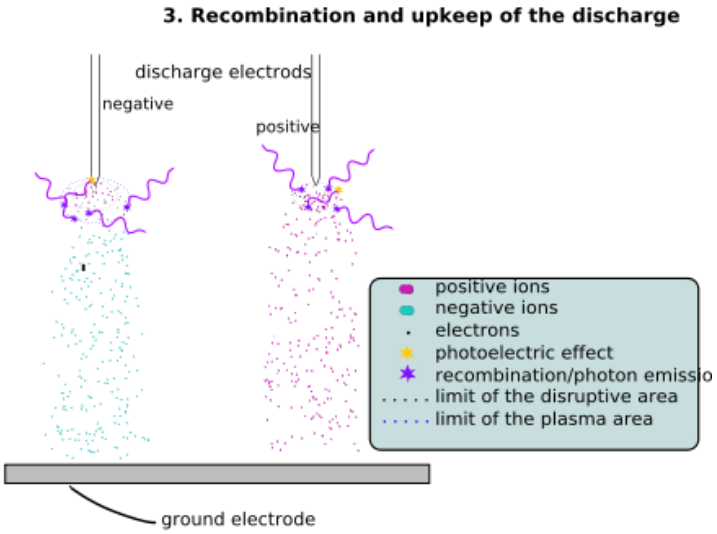

Fig. 8 (Public domain).

Negative corona discharges are only created in mediums with a high density of electronegative molecules (O_2, CO_2, H_2O, etc.) to receive free electrons and sustain the electron avalanche. Without enough electronegative molecules, negative ions cannot form and the charge buildup on the electrode will eventually become a spark (Beggs, 2006). In our study, the predominant phenomenon is the positive corona discharge: In positive coronas, the free electron density is much smaller (a thousandth) than in a negative corona, but they are very close to the electrode surface and so they have very high energy. These high energy electrons are a priority for ignition applications, so positive corona discharge will be treated as the standard from here on.

Additionally, the separate positive and negative particles are propelled by the electric field, producing a stream of charged particles, known as ionic wind. This phenomenon can be used in various applications such as:

- Fanless (solid state) convective cooling systems
- Means for propulsion
- Drag force reduction
- In the case of an ignition system, to generate turbulence near the surface of the electrode.

4.3 Research

The main improvement for corona discharge ignition is reflected in the results presented by Bellenoue et al. showing that there is a dramatic increase in combustion speed brought by a volume ignition. This has many implications.

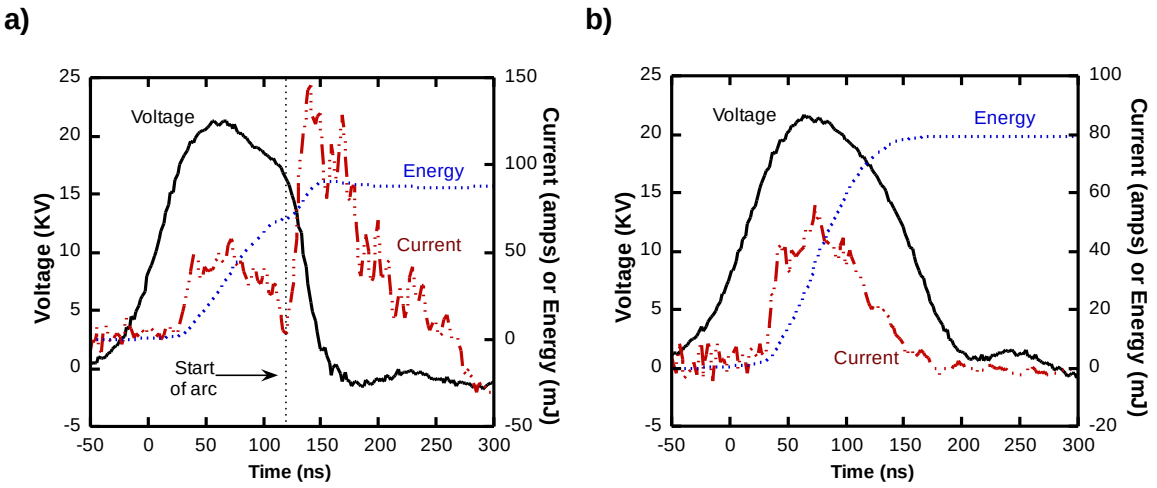

Fig. 9 Comparison of the power consumed (current over time) by the medium using an a) Arc and b) Corona discharge ignition (Ronney, 2004).

There are two key parameters in assessing an ignition device; first, the ignition delay time, which is the required time to achieve 10% of the pressure high; second, the rise time, which is the required time between 10%-90% of the pressure increase. In corona discharge ignition devices, they are both reduced by a factor of approximately 3 (Ronney, 2004). Furthermore, faster combustion produces a higher peak pressure as well as lower heat losses (Ronney, 2004).

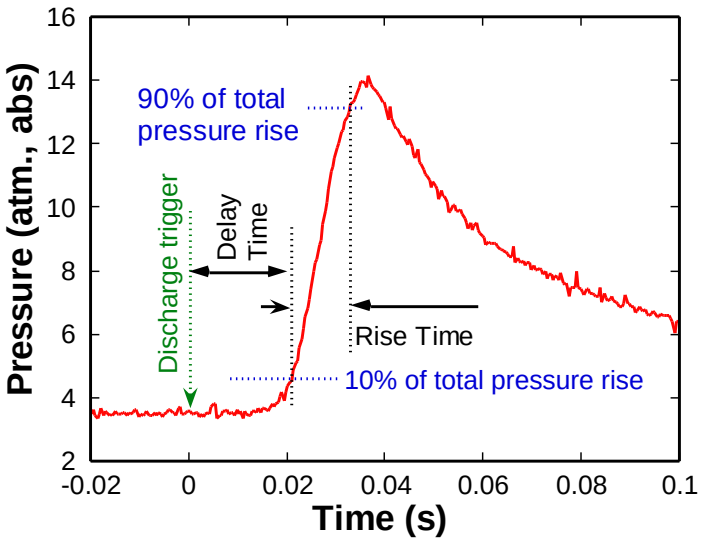

Fig. 10 (Ronney, 2004).

This improvement is accentuated when the mixture ratio decreases, i.e. there is an abundance of oxidizer (air) relative to the fuel's oxygen requirements. The combustion time decrease using corona discharge is larger for lean mixtures ($\phi < 1$) than for stoichiometric mixtures ($\phi \approx 1$) (Bellenoue, 2005).

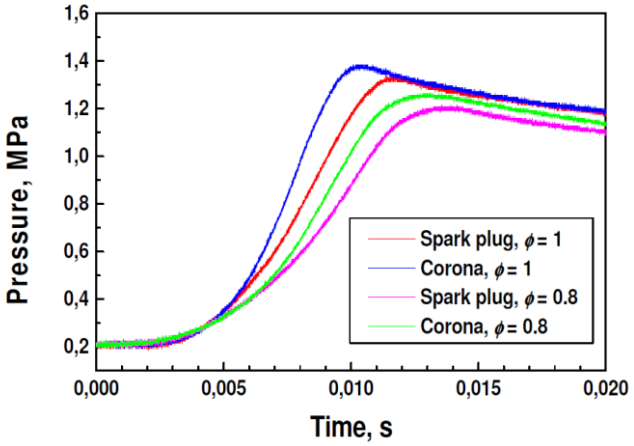

Fig. 11 (Bellenoue, 2005).

Lean-burn engines have improved efficiencies by reducing throttling losses and allowing higher compression ratios. By allowing combustion to occur with excess air, HC and CO emissions are drastically reduced, but at the cost of high NOx levels. Currently, to clean the exhaust gases of NOx a complex catalytic converter is needed. However, as exposed by Jan Vinogradov et al. the same corona discharge technology can clean the NOx from the exhaust gases (Vinogradov, Rivin, Sher, 2006).

The faster pressure increase produces a 25-40% faster combustion, depending on the mixture, as another study suggests. This is mainly due to three factors:

1. Greater turbulence created by ionic wind. Wind speed of 4-6m/s and 0.8-1.2m/s turbulence, depending on the number of streamers[3].
2. Not losing as much heat through the cylinder walls.
3. Larger ignition volume (Bellenoue, 2005).

[3] Streamers are the corona discharge ionization plumes that emanate from each geometric sharp tip or edge. Thus, each electrode may have one or several streamers.

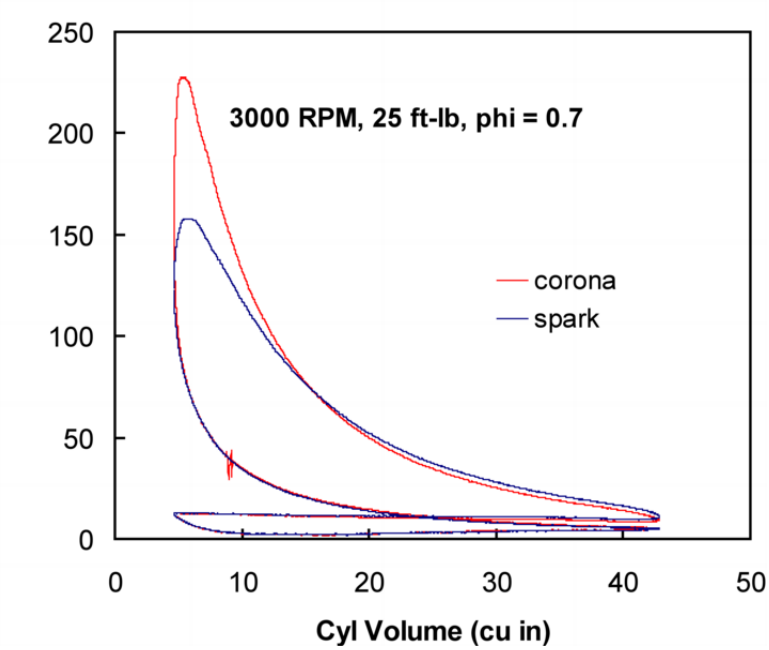

Fig. 12 Note the indicated mean effective pressure increase in a four-stroke engine (Ronney, 2004).

Sparks have a very limited volume of interaction with the medium to ignite, spend most of their energy in simply transferring charge from the anode to the cathode and generate a wasteful amount of light and sound. This reflects poorly in wall-plug efficiencies, as the energy required to ignite a punctual volume of mixture is much smaller than the energy used to produce the spark. Corona discharge being a high-energy volume ignition can achieve wall-plug efficiencies over 50%, as it produces less light and noise compared to an arc with the same energy deposition (Ronney, 2004).

The volume of ignition is tightly related to the corona gap[4], as well as the aforementioned streamer properties. Consequently, the corona gap is a parameter which when increased, augments the volume of ignition and causes faster combustion and pressure increase (Bellenoue, 2005).

[4] The corona gap is the distance between the tip of the electrode and the grounded surface.

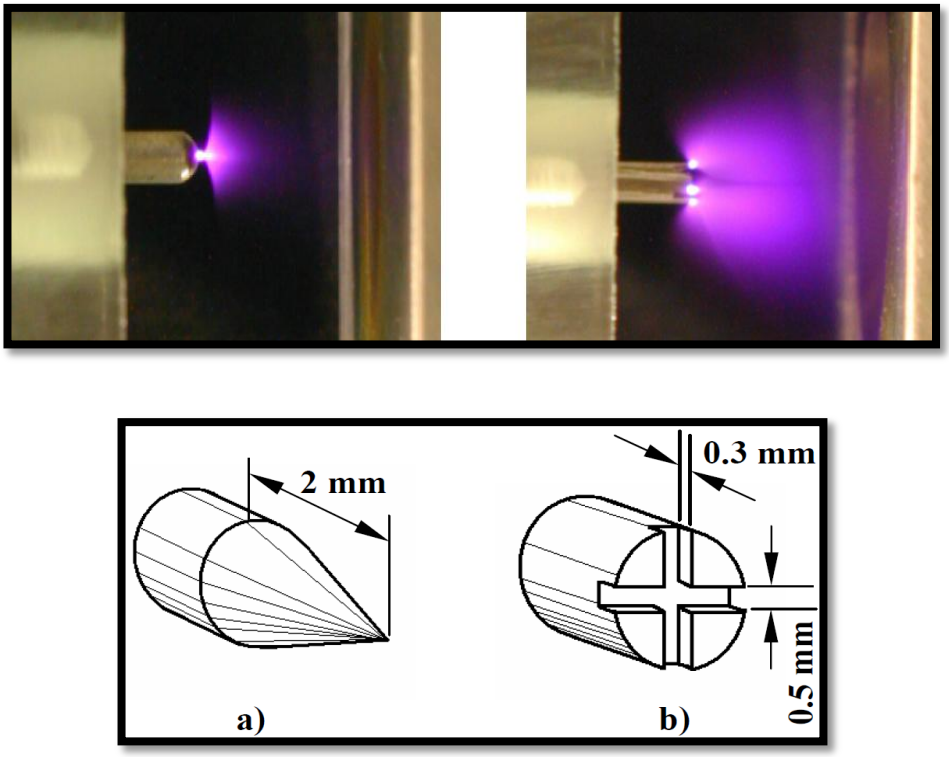

Fig. 13 The purple plumes show the space with highest medium ionization. Note how an electrode with a greater amount of sharp points and edges will create a greater area of influence (Bellenoue, 2005).

Furthermore, corona discharges not only transfer more energy into the ignitable medium but simultaneously consume less energy. The energy consumed is in the order of 10 times less in corona discharge compared to spark (0.8-1.2mJ vs. 10-12mJ), depending on mixture ratio (Bellenoue, 2005).

This high wall-plug efficiency depends on the field strength and polarity alternating frequency. It has been found that the most efficient energy delivery into the medium is achieved at 4kV/cm and under 1kHz (Vinogradov, Rivin, Sher, 2006). However these measurements taken in the exhaust pipe have a very strong correlation to the medium's pressure, density and contents, and so, although a good starting point, it will be regarded only as a pointer for ignition applications in our tests.

4.4 Environmental considerations

Internal combustion engine designs aim at being more energy efficient and consuming less fuel. This has been a constant trend for several years, and until recently this objective had a merely economical motive. But increasingly, people are growing aware of the pollution produced by internal combustion engines (especially cars) and how it may have a significant negative effect on health.

Public opinion and health issues have been read by policy makers and consequently emission limits have consistently been growing ever more restrictive in favor of a healthier environment (Commission Regulation (EU) No 582/2011, 2011). Five substances are currently monitored by the EU Emission Standards: Carbon monoxide (CO), unburnt hydro-carbons (HC), nitrous oxides (NOx) and particulate matter (PM) all in g/kWh, number of particles (PN) in units/kWh, and smoke in visibility m^{-1}. The limiting, taxing and overall monitoring of emissions places manufacturers' power train departments under a lot of pressure to innovate and use new technologies not only to be more economically sensitive and more energy efficient, but also to be cleaner.

Both carbon monoxide (CO) and unburnt hydrocarbons (HC) are a direct consequence of an incomplete combustion. By using a corona discharge for high energy volume ignition the engine will have reduced the fraction of unburnt fuel (HC) and will have equal or less Brake Specific NOx emissions (Ronney, 2004).

This significant improvement comes at the cost of higher NOx emissions. Paradoxically enough, corona discharge can also play a role in cleaning NOx after combustion as demonstrated in an exhaust pipe emissions cleaning device described by (Vinogradov, Rivin, Sher, 2006).

In this exhaust cleaning corona discharge device, some interesting results were obtained. Previous works provided the values of energy needed for decomposition of 1 g of NOx of 0.04[kWh/g-NOx] for wire-to-duct pulsed corona, 0.067[kWh/g-NOx] and approximately 0.1 [kWh/g-NOx] for coaxial cylindrical pulsed corona (Vinogradov, Rivin, Sher, 2006).

4.5 Ignition in flux engines

Ignition in flux engines is only strictly necessary during engine start. After that, the flame holders create the thermodynamic conditions for the mixture to ignite spontaneously due to the increased pressure and heat generated by the continuous flow.

It is advised to turn on the ignition device in turbines during adverse conditions and especially during landing. These devices are diverse, but invariably generate a spark at regular intervals.

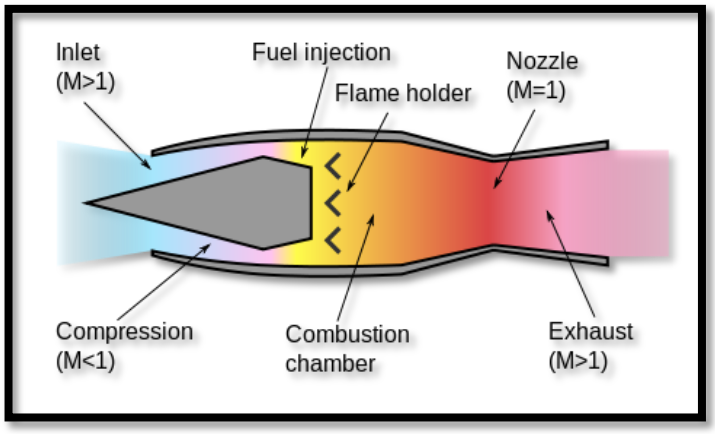

Fig. 14 Ramjet diagram. The compression required in the thermodynamic process is achieved without a rotary compressor, but with a geometrically specialized intake and high speed (> Mach 1). These engines operate efficiently at Mach 2-4 (MIT - Unified Engineering).

The full extent of applications for corona discharge ignition in gas turbines has yet to be investigated. However, there are at least two interesting research leads.

In supersonic aircraft ram jets, ignition and flame holding at high altitudes is an important technological challenge. By simply being at high altitudes, a low-volatility fuel must be used (such as JP-7[5]). Its flash point is increased, i.e. a higher required temperature for ignition, or

[5] JP-7 is a military-grade fuel composed primarily of hydrocarbons, including alkanes, cycloalkanes, alkyl benzenes, indanes/tetralins, and naphthalenes, with addition of fluorocarbons to increase its lubricant properties, an oxidizing agent, and a cesium containing compound, which disguises the radar signature of the exhaust plume. It contains less than 3% of highly volatile compounds and very low quantities of sulphur, oxygen and nitrogen impurities.

greater energy transfer is required from the ignition source by the fuel. Especially, during engine start.

In the past this has been solved by using auxiliary highly flammable substances (e.g. triethylborane, or TEB) that will ignite merely by coming into contact with oxygen, to start the engine and heat it to a point where a low volatility fuel can be used.

Corona discharge ignition may present advantages in adverse ignition conditions, as well as producing a cleaner exhaust. Especially for high relative emission (g/MJ) fuels.

Fig. 15 The iconic SR-71, whose turbojet engines work as ramjets at speeds over Mach 1.

4.6 Federal-Mogul Patent US 20130208393 A1

During the state of the art investigation, this patent was encountered. It describes a self-tuning power amplifier which is designed to provide a high frequency high voltage electrical signal to a corona discharge electrode.

Application number US 13/842,803

Publication date Aug 15, 2013

Filing date Mar 15, 2013

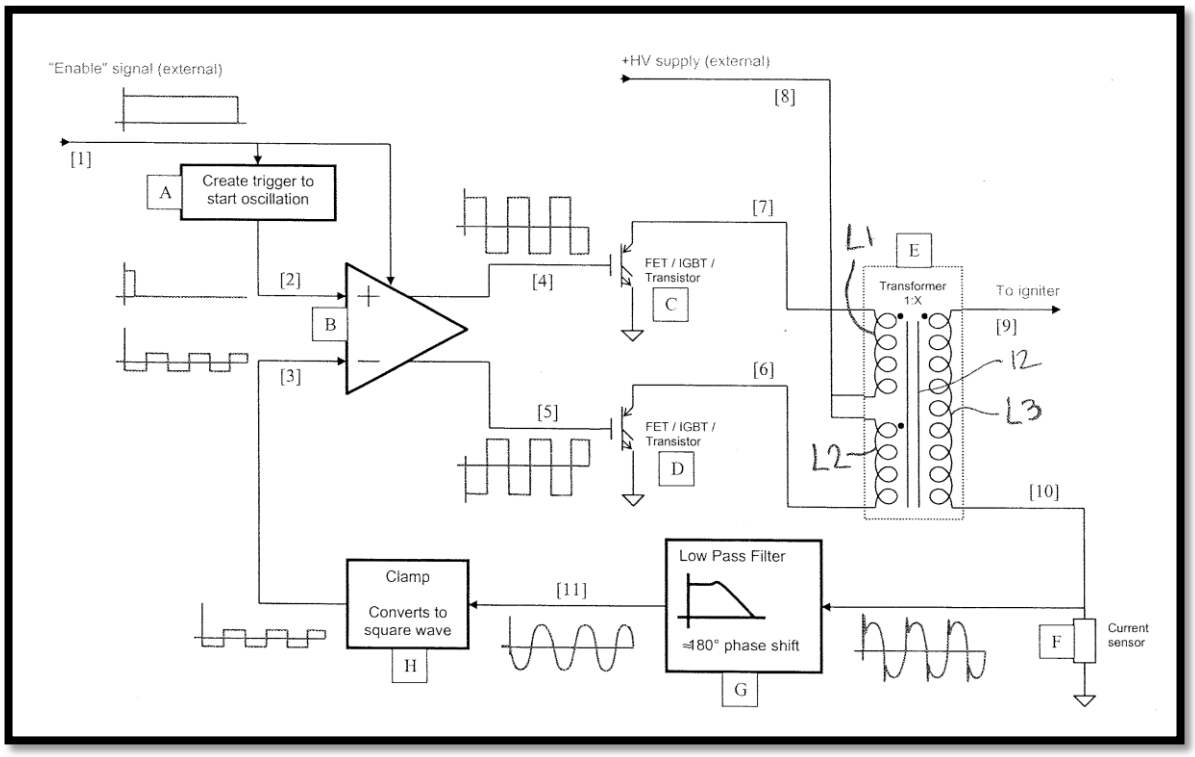

Fig. 16 Concept of the Advanced Corona Ignition System's electric circuit.

In an Otto cycle engine, as the compression stage is completed, the enable signal is triggered. "A" indicates the amplifier to start emitting two opposite AC square signals. These signals alternately open and close a high voltage rail, driving currents through two primary coils wound around the same iron core. This magnetic field variation has a transformer effect on the secondary coil, which elevates voltage. The secondary coil then carries the high voltage lead to the electrode and is also filtered and used as feedback to establish the oscillating frequency for the amplifier. This feedback system allows the device to operate at the highest possible frequency for the resonant circuit.

This circuit creates a high frequency alternating current that has a very short transient state until reaching stationary high frequency resonance.

5 Experiments

5.1 Data acquisition

5.1.1 Equipment

5.1.1.1 High voltage probe

Fig. 17 Above, image of the high voltage probe. Below, use information.

A hook was crewed on the tip in order to allow it to hang from a hole in the transformer lead, for easy assembly.

The ground connector was left floating as the voltage is measured relative to the ground of the oscilloscope and the transformer.

This probe provided the real applied voltage difference between the transformer's leads. The measured voltage is divided by 10^3 in order to make it compatible with an oscilloscope channel input, which is limited at 300V.

5.1.1.2 Oscilloscope

Fig. 18 Image of the oscilloscope's screen and controls with the high voltage probe and a BNC cable connected.

This oscilloscope Tektronix TDS2002C will register the measurements. It is capable of recording data directly into a USB drive.

5.1.1.3 High voltage transformer

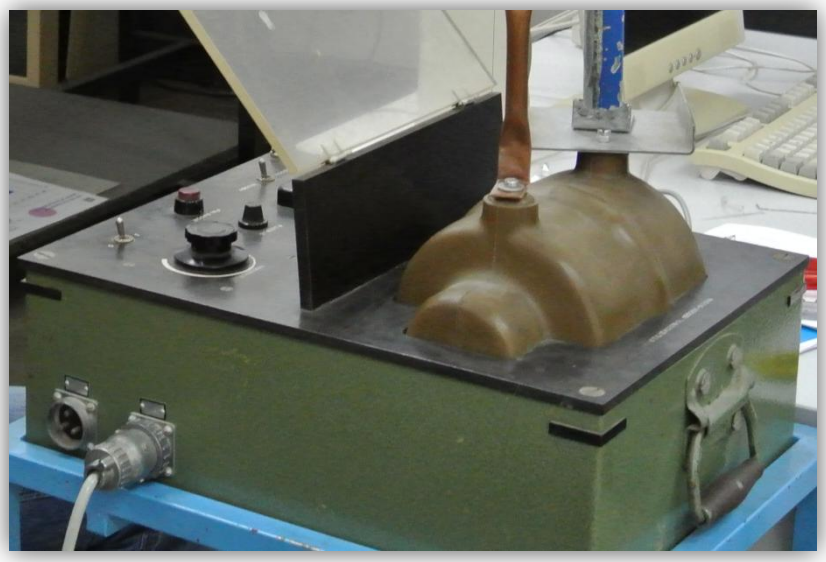

Fig. 19 High voltage transformer for rigidity tests. The output can be regulated and has a maximum output of 15kV, visible through an analog dial. The input is the mains plug, 230V 50Hz. The output is protected by a fuse and a breaker switch, in case of short-circuit. Its internal resistance is 6kV.

The current throughput will be measured with a shunt resistor. The design of this shunt resistor is a key factor in obtaining useful data. The partial discharge phenomenon produces high voltage and must be sampled at high frequency, which poses the following issues for measurement:

1. High sampling rate required. This oscilloscope is capable of digitally recording 10^9 samples per second. This would sample signals up to $5 \cdot 10^8$, according to Shannon's Law, but would produce significant error, especially in peaks.
2. High voltage. Corona discharge can develop into an arc, which completely ionizes the medium, short-circuits the dielectric's resistance and causes the current to peak. This causes a voltage surge to the measuring device which can destroy it. The shunt resistor will be designed to meet these safety requirements. As for the input voltage, the high voltage measurement is solved by using the provided high voltage probe, which divides the measured voltage by 10^3, down to a safe voltage level.

5.1.1.4 Soldering iron

Fig. 20 The used soldering iron.

The soldering iron is relevant in the construction of the high frequency shunt resistors and electrodes.

In the initial attempts, an electronics soldering iron was used, with a rated power of 25W. The solder didn't correctly adhere to the copper plate surfaces because the temperature was too low.

The second soldering iron (pictured) has an input power of 70W. This soldering iron does not necessarily reach a higher temperature than the first one with a lower power, but will enable soldering onto bodies with high heat capacities or high dissipation, such as the copper foil used for the high frequency shunt resistors.

5.1.1.5 Nikon 1 J2 camera and Nikkor optics

For specialized imaging, the Nikon 1 J2 camera body was used, in combination with the Nikkor 10-30mm focal distance, f/3.5-5.6 aperture lens.

This camera allows the user to control exposure time, aperture and ISO sensitivity up to an extent similar to a professional SLR camera.

Although it is an entry level mirrorless interchangeable lens camera, it allows to take high exposition photographs, up to manually controlled time intervals, as well as to record high speed video up to 1250 frames per second.

Fig. 21 Images of the body of the camera (left) and the lens (right).

A small articulated tripod stand was also used for long exposition photography.

5.1.1.6 Point-Point electrodes

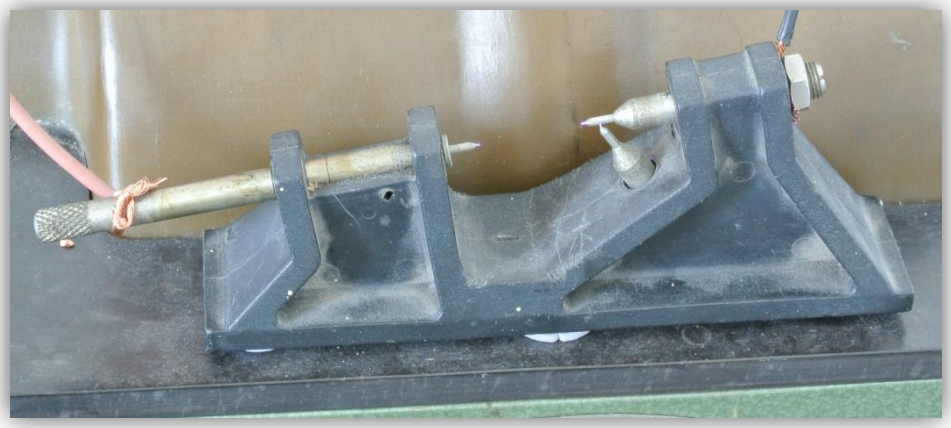

Fig. 22 The plastic support holds the electrodes' tips at a variable distance.

In order to generate arcs and to avoid premature destruction of the electrode tips, a specialized instrument was used. The material the tips are made of is designed to sustain high temperatures and electric erosion.

These electrodes and support were also used to measure corona discharges from point to point electrodes.

One of the electrodes is not fixed in order to increase or decrease the separation distance between the tips.

The third tip, oriented at an angle, was not used in this study.

5.2 Preliminary experiments

5.2.1 Setup #1

With the first setup, the objective is to generate corona discharge using materials readily available in the lab.

The main objective is to design a system with variable capacitance, in order to analyze the effect of increasing capacity to medium breakdown.

A concentric cylindrical capacitor was built, consisting of:

- Acetate film as dielectric
- Aluminum foil
- Spring steel wire for slide tube contact

Fig. 23 Sliding concentric capacitor tube. The visible aluminum contacts the opposite pole using the wire.

Fig. 24 Overview of the setup.

The dielectric with the aluminum foil is inserted over the copper tube and the wire contacts the other pole of the transformer.

At 500V the corona discharge is audible.

In low light a faint blue glow can be seen.

At around 6000V the dielectric acetate film was perforated, producing a hole in the dielectric and rendering the condenser unusable.

The range at which the discharge can be heard and seen did not change.

This configuration demonstrated that partial discharge was not affected by the capacitance between electrodes: The partial discharge always occurs at the edge of the aluminum foil and the inside copper tube, independently of the overlapping concentric conductive cylinder area.

This confirms that the partial discharge phenomenon is a consequence of high electrical field gradient and not capacitance.

5.2.2 Setup #2: Imaging

Fig. 25 Image of the setup with the fixed camera on a stand for long exposure photography.

The goal is to record the visual display of the corona discharge.

The phenomenon is visible at plain sight in low light, but it is very faint.

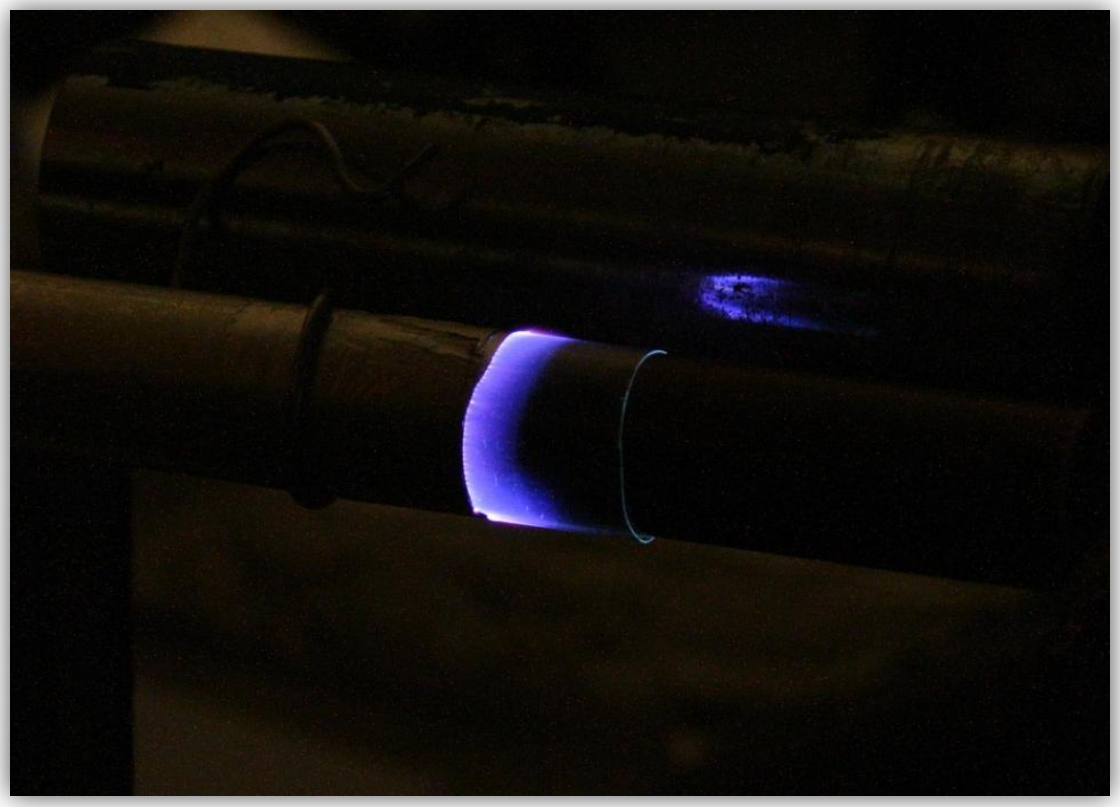

Fig. 26 Long exposure photography captures the photons emitted by the ionization of the medium surrounding high gradient areas.

This image was taken at a 5500V, acetate dielectric thickness of 0.08mm. Exposition time was 30 seconds, f5.6 aperture, and sensitivity ISO 400.

The corona discharge is clearly visible at plain sight but it is best captured in long exposition imagery.

The plume exits the edge of the outer aluminum foil (sharp edge) along the dielectric, towards the inner copper cylinder.

It cannot be seen in this picture but a similar corona discharge is simultaneously happening in the inside edge of the inner (copper) tube. The voltage range between first corona discharge electron avalanche and arc is widened; in this case it is between 500V and 6kV, approximately.

5.2.3 Setup #3: Data Acquisition

To measure the transmitted current, a shunt resistor was constructed. However, since it is fundamental not to lose detail in the acquired signal, it was designed to reduce noise created by inductive-capacitive effects at high frequencies.

The following pictures correspond to the first version.

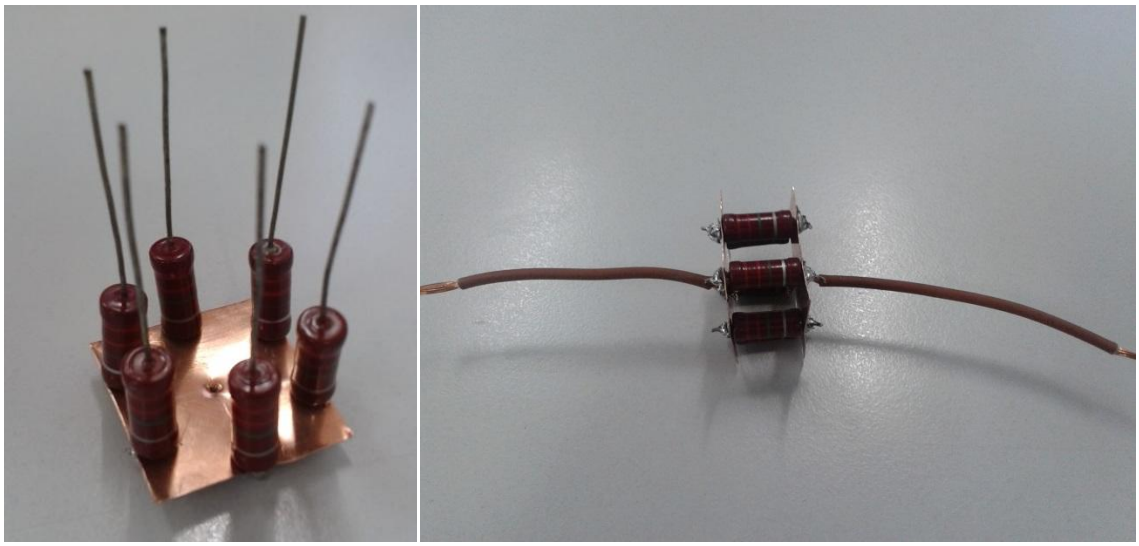

Fig. 27 Image of the shunt resistor, while it was being built (left) and finished (right).

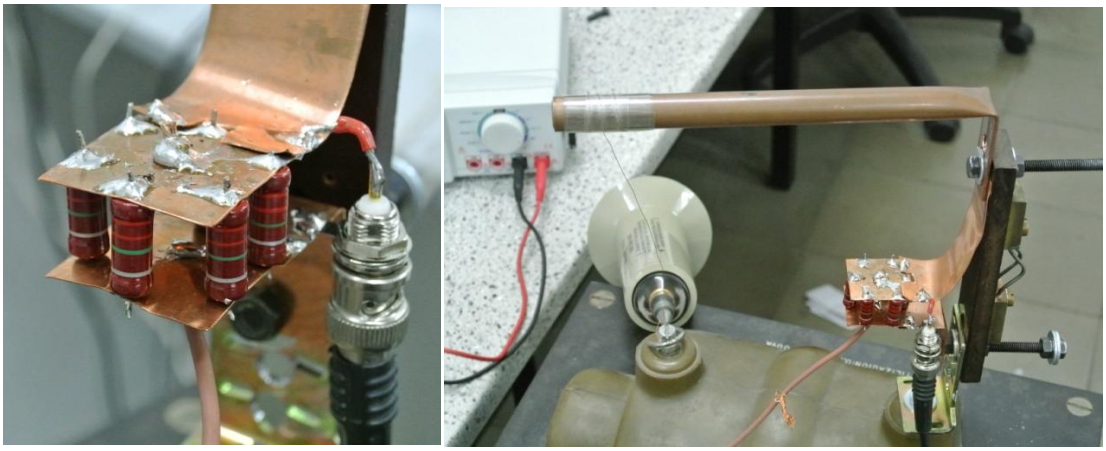

Fig. 28 Image of the shunt resistor with the BNC connector soldered to the side (left) and built into the copper plates (right).

A copper plate was used instead of wire to reduce inductive effects. The resistors were placed coaxially to the lead of the BNC connector for the same reason. All sharp edges were dulled to avoid loops and capacitive effects.

These recommendations were extracted from procedures followed to probe high frequency and high voltage signals, and are described in various articles by Dr. Fernando Garnacho Vecino.

This design allowed us to produce corona discharge and to measure its current output on an oscilloscope, although the shunt resistor probably wasn't effective in reducing the high frequency noise, especially by not being coaxial and not having rounded sides

A copper wire was wound around several layers of the same acetate film, around a copper tube. A 4.2kV amplitude and 50Hz electrical signal was used. This voltage was fixed by hearing a significant crackling noise originating on the wound wire, but low enough not to perforate the acetate with an arc.

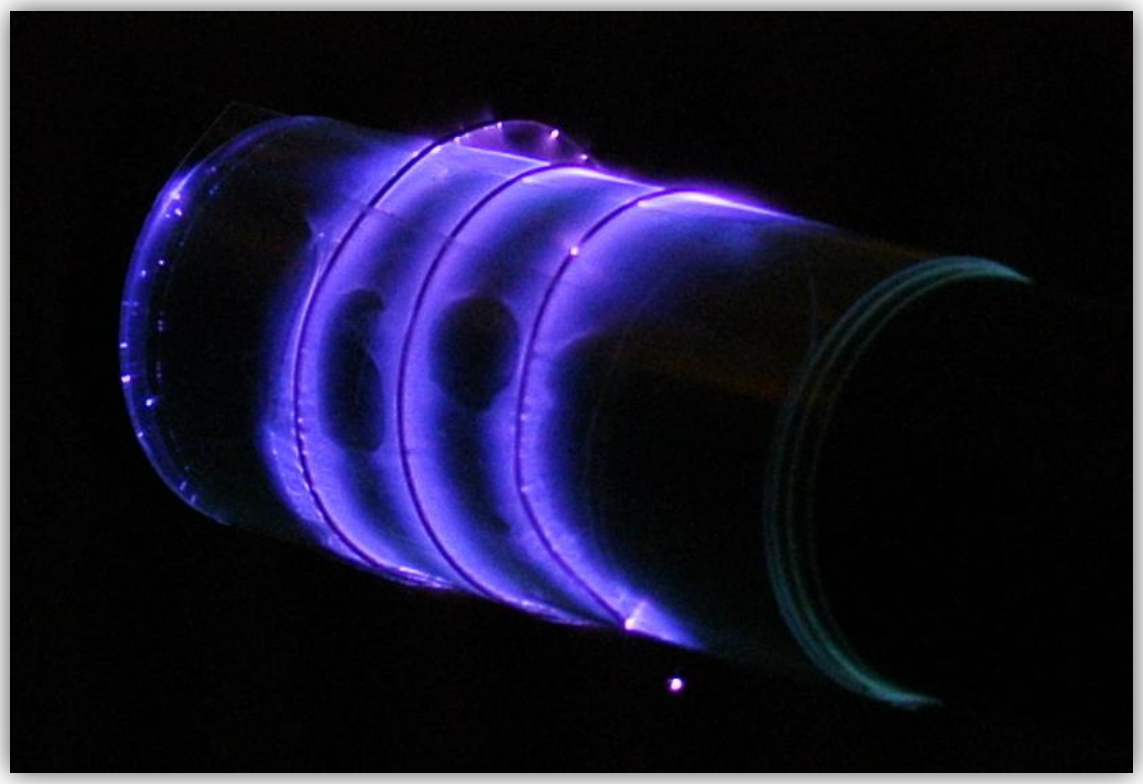

Fig. 29 Long exposure image taken from the second setting.

The corona discharge occurs on the ø0.25mm copper wire. This image was taken with a 28mm focal distance, f5.6 aperture and 30 second exposure time. Note how the small imperfections on the wire produce the accumulation of field gradient, thus appearing brighter.

The electrode was not intended to create an area of influence suitable for a mixture flux and ignition, but for preliminary measurements.

The high frequency shunt resistor used in this test has a measured resistivity of 379.4kΩ, that is, 379.4V/mA.

Using the data sampled with the probes and recorded with the digital oscilloscope, a graph was plotted to visualize the measures.

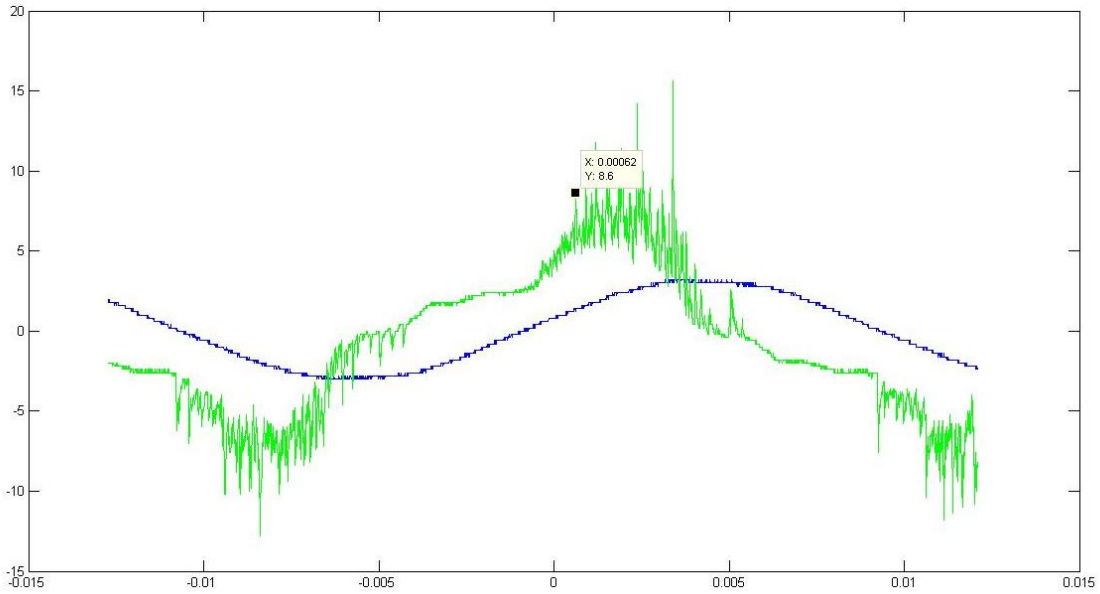

Fig. 30 Graph from the data recorded by the oscilloscope. The applied voltage (in blue) has an attenuation factor of 1000, so it has 3kV of amplitude. Colored green is the shunt voltage drop.

The first positive distinguishable spike in the output was selected (marked) for measuring the emitted power. This one was selected because it was large enough to be distinguishable, but small enough not to incur in too much error, as the sampling rate is not high enough at this scale.

$$E = \int_{t1}^{t2} (V_{shunt} * \frac{1mA}{379{,}4V}) * V_1 * 1000\ dt \qquad \text{(Eq. 1)}$$

The result of integrating along time by the trapezoidal method is **1.7681e^{-2}mJ**.

The lowest ignition energy value occurs at the stoichiometric combustion concentration. For most materials this can be calculated from the carbon and hydrogen content. For gasoline, the MIE is 0.8mJ (Babrauskak, 2003), however ignition devices are designed to generate 10-100 times more energy than what is strictly necessary to ensure ignition.

5.3 Point-plate experiment

The following version produced a design that integrates the shunt resistor, probe and electrode in one single piece.

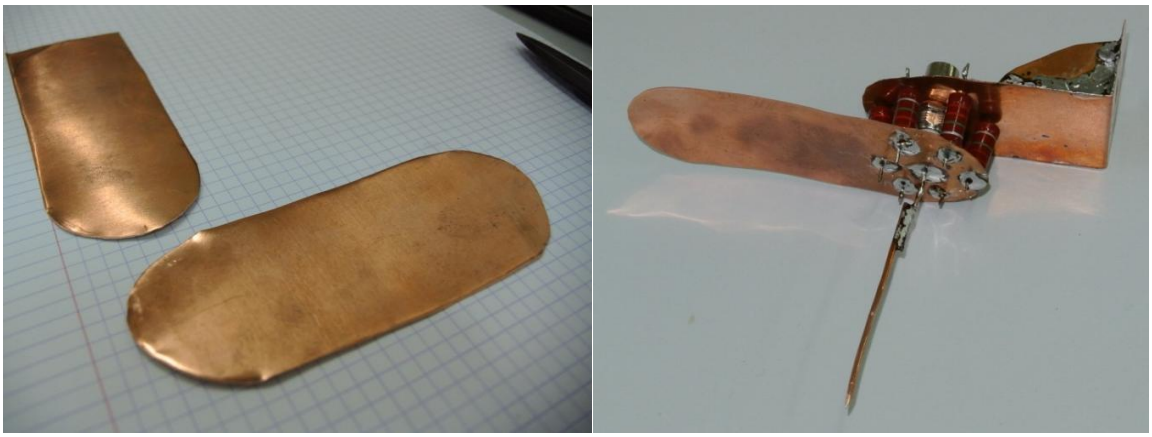

Fig. 31 The shunt resistor and electrode built. Left, the copper plates cut, onto which the BNC connector, resistors and support structure was built. Right, the shunt resistor and electrode before the final trimmings.

Copper foil, 0.25mm thickness, preliminary cutting. The foil is used over cable to reduce inductive effects.

Six 2.2MΩ 10% tolerance resistors were soldered in a hexagonal arrangement around the BNC connector. The electrode was made out of a 1.8mm solid copper wire. The wire was soldered to the lead in the center of the secondary copper foil.

By placing the resistors in a coaxial pattern around both the sensor and the electrode, this shunt resistor will reduce the inductive effects, and the resulting noise, in high frequency measurements.

Kneaded rubber was added to the electrode side of the device. This prevents the rest of the device's surface to produce high field gradients and acting as an electrode, by greatly increasing the dielectric constant on the surface of the metal. The generated field on the surface of the metal will be significantly reduced, and will leave the electrode tip as the main geometric region for high spatial gradient.

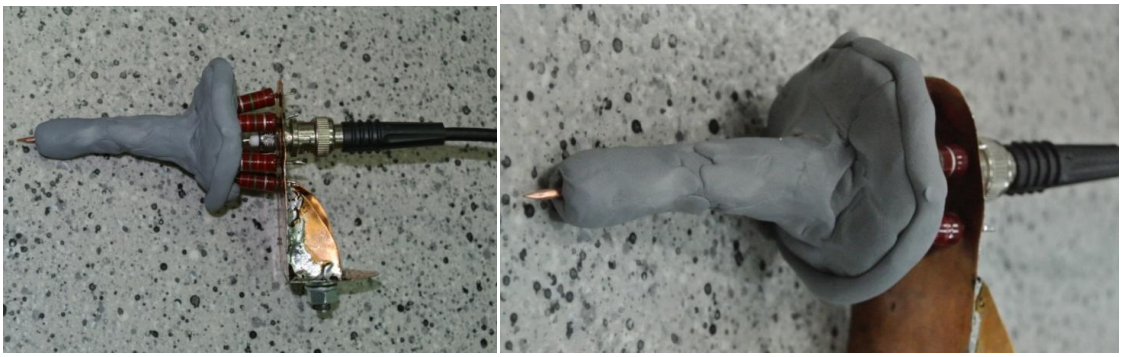

Fig. 32 Two views of the finished shunt resistor and electrode with the BNC cable connected (left). All of the surface facing the opposite pole is covered in kneaded rubber, and is used to minimize the effect of electrical field gradient outside the electrode tip, left uncovered (right).

5.3.1 Electrical circuit

The following electrical circuit was used to model all of the settings:

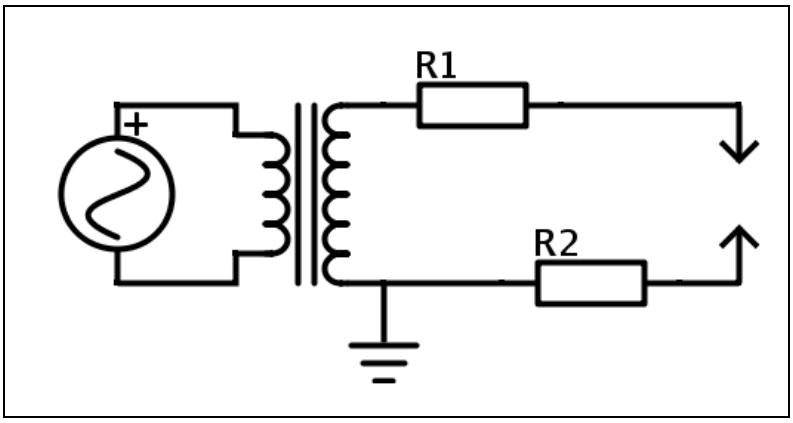

Fig. 33 Electrical circuit used as a model for all settings.

In this scheme, R1 is the internal resistance of the transformer and R2 is the value of the shunt resistor.

The measurements were done as follows:

- The high voltage probe was connected between the transformer's internal resistance and the tip of the electrode in the model circuit. The ground was established by the ground lead in the oscilloscope.
- The shunt voltage drop probe was always built with the positive lead on the electrode end of the resistor. The ground was the other end of the shunt resistor and connected to the ground in the oscilloscope.

This setup causes both the high voltage and low voltage measurements to be sampled inverse to what the relevant measurement is. The high voltage probe will indicate the voltage of the opposite lead to the shunt and the low voltage probe will indicate the voltage at the tip of the electrode as the higher value.

These construction restraints are taken into account by multiplying each sample by -1 from here onward.

5.3.2 Acquired data

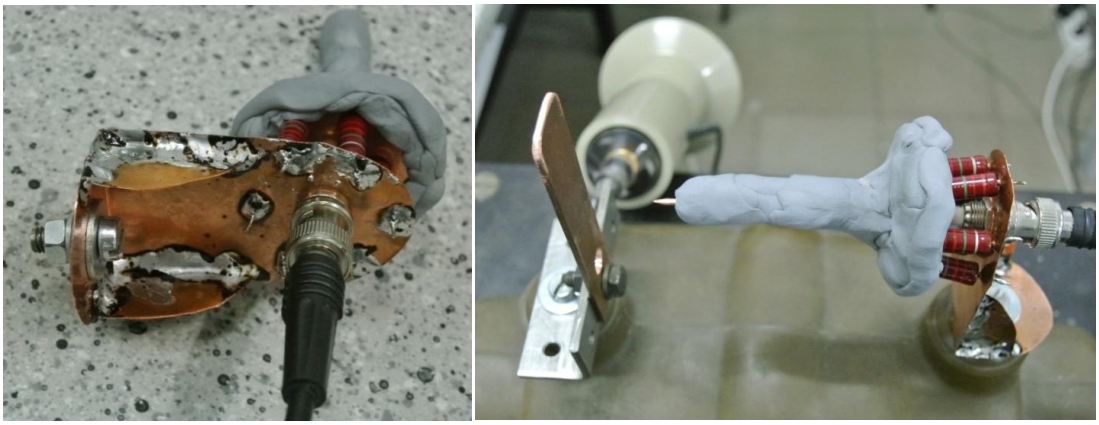

Fig. 34 Left, detailed view of the soldered resistors, BNC connector and structural support. Right, the point-plate setup, mounted on the transformer, ready for measurements.

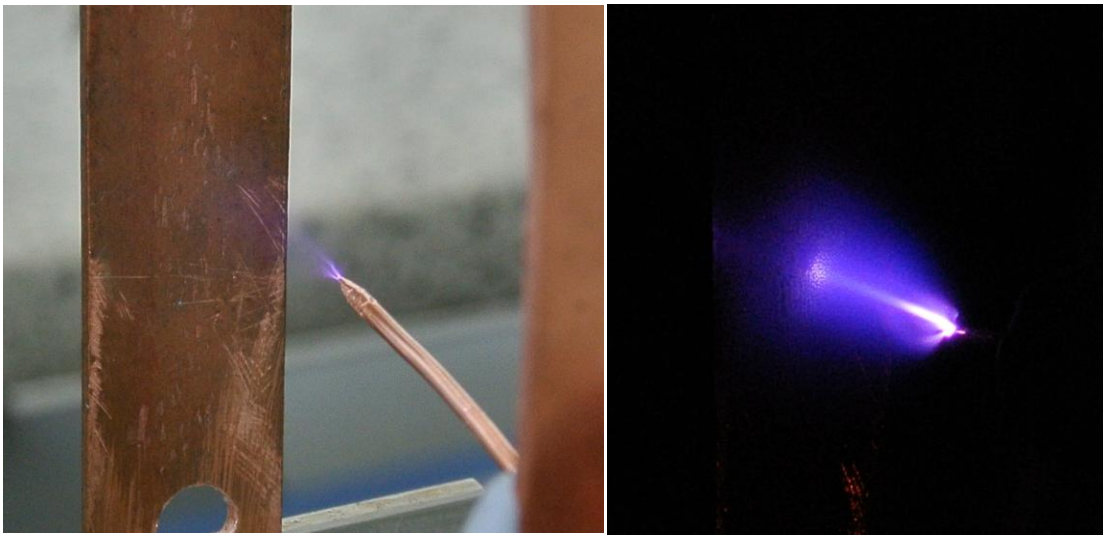

Fig. 35 Left, long exposure image in daylight. Right, long exposure image in very low light. Note how the area of influence resembles a cone, with the vertex on the electrode tip, with a much higher brightness in the axis of the cone.

In this setting the oscilloscope reveals the differences between positive and negative input voltage polarities. This is due to two factors: the distinct curvature radius of the two poles; one is sharp (very small curvature radius) the other is flat (infinitely large curvature radius); and the resistance to ionization of the medium depending on polarity.

For all of the following measures, the shunt resistor used to calculate the current was 356V/mA.

The separation between the electrode tip and the plate was fixed at 20mm.

5.3.2.1 6kV

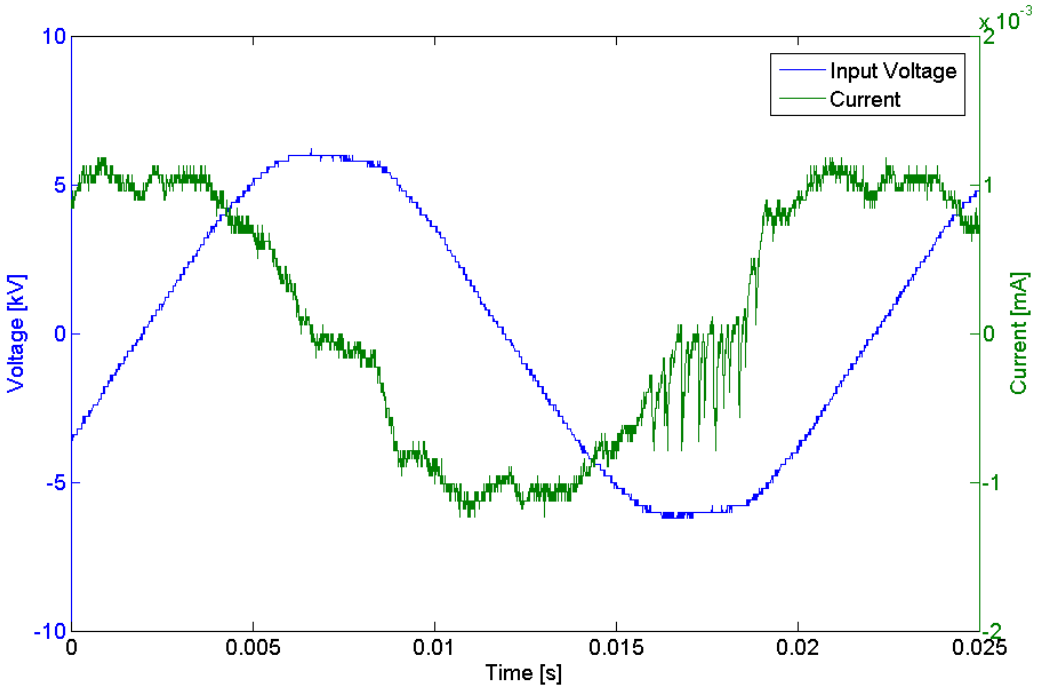

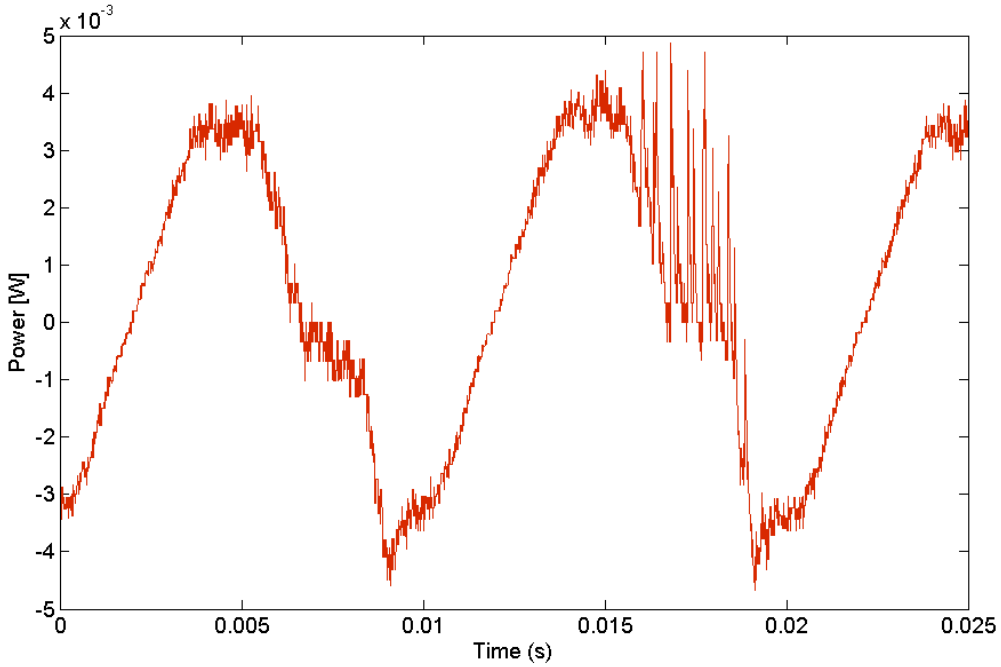

V_{IN}	I_{max}
6kV	~1.12E-6 A

The current is offset π/4 from the input voltage. This is because the dielectric between both electrodes acts as a capacitor. This current is actually the sum of two wave signals: capacitive and conductive current.

There is electrical charge transfer taking place between the electrodes. This is reflected in the 50Hz sinus wave which can be seen, albeit noisy.

In the current graph, corresponding to the negative peak in input voltage, there is a ripple in the current intensity (green) signal. This ripple reflects the phenomenon of dielectric barrier discharge (van Veldhuizen, Rutgers, 2001). This ripple corresponds to the sinus wave signal of the conduction current, which at this applied voltage is incipient.

5.3.2.2 7kV

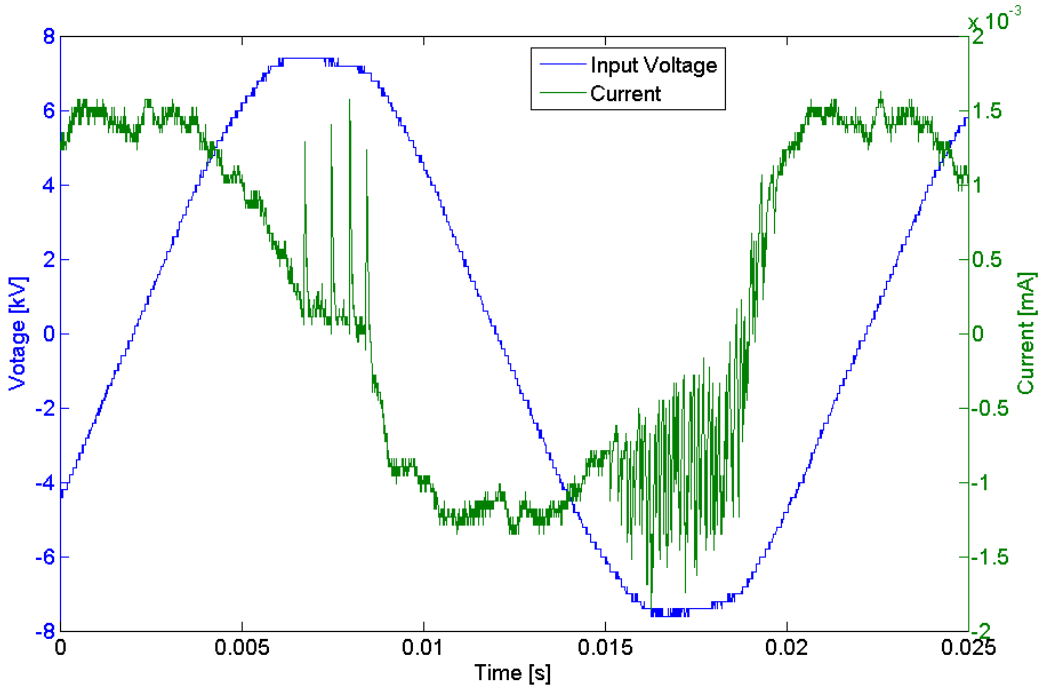

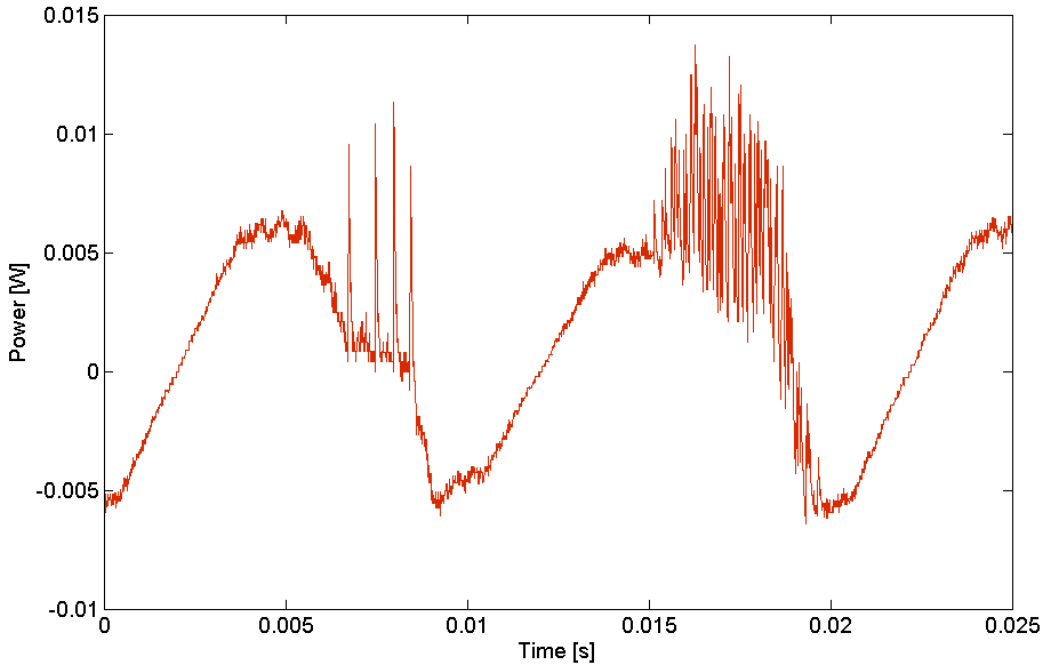

V_{IN}	I_{max}
7kV	~1.5E-6 A

Compared to the previous graph, the dielectric barrier discharge has increased along the negative semi-period of the input voltage and has started to be visible in the positive semi-period.

This incipient discharge will be referred to as capacitive current from here on.

The capacitive delay of the current is still clearly distinguishable.

5.3.2.3 9kV

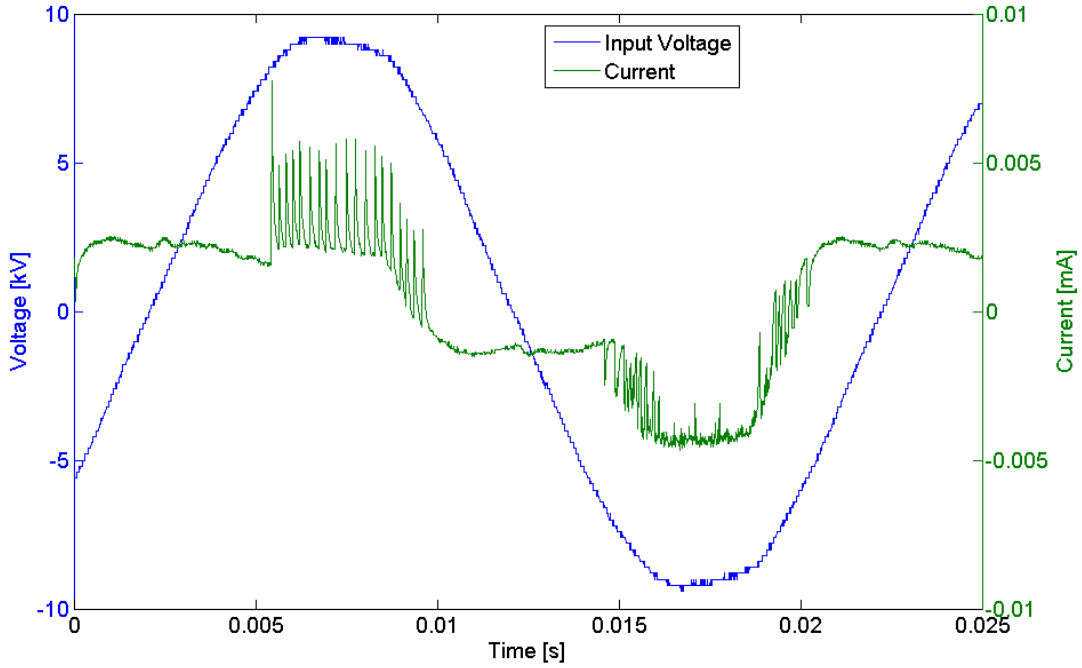

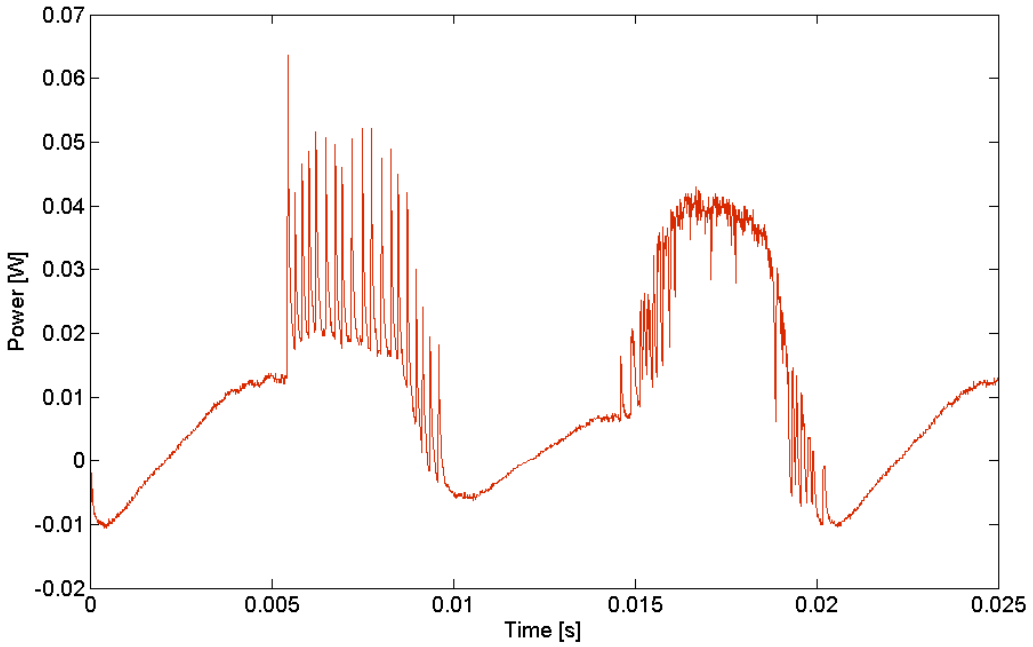

V_{IN}	$I_{capacitive}$
9kV	~6.4E-6m A

In this still, both the conductive and capacitive current wave signals are clearly visible. The conductive wave signal is synchronous with the voltage input and the capacitive signal is offset 90º.

The conduction signal corresponding to the dielectric barrier discharge is asymmetrical. The positive semi-period can't establish a constant conduction and produces many tightly packed peaks.

5.3.2.4 12.5kV

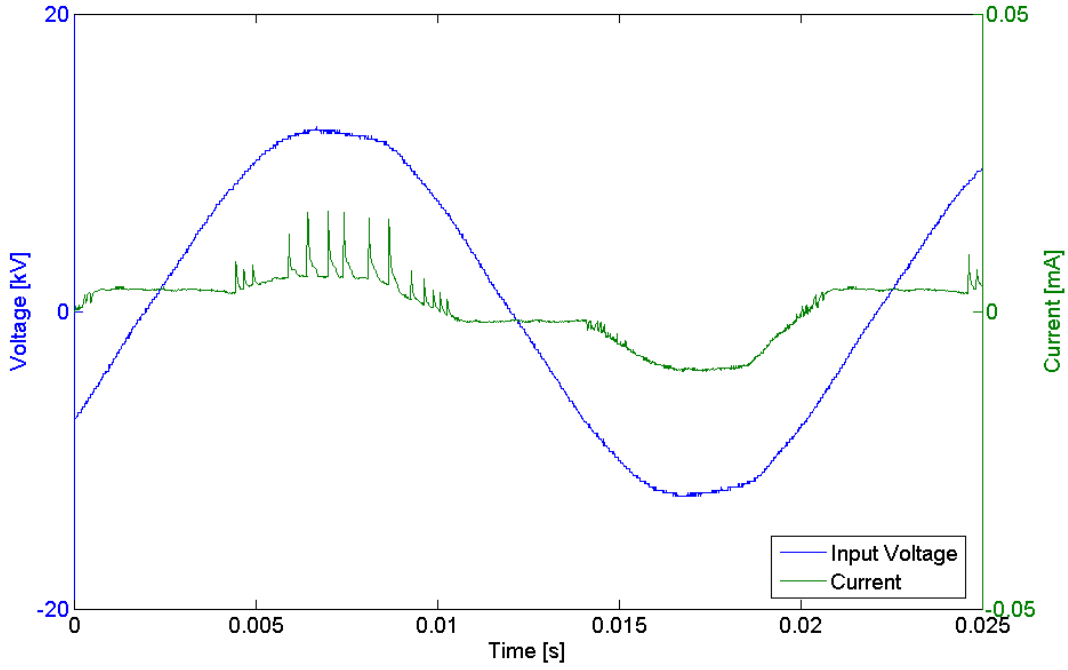

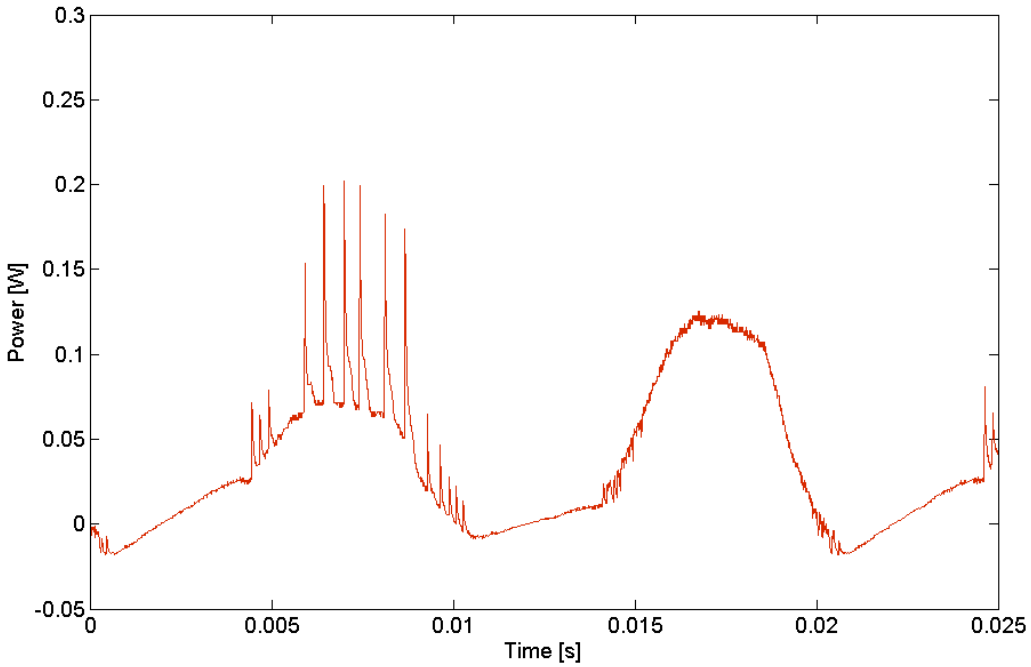

V_{IN}	$I_{capacitive}$
12.5kV	~2E-5 A

From this measurement on, the capacitive delay attributed to the dielectric between electrodes can no longer be seen, and is completely substituted by the continuous conductive and the chopped capacitive currents, synchronous to the input voltage.

This indicates that the dielectric barrier cannot resist the ionizing electric field and consequently yields to the conduction of charge.

However, there is no arc discharge. Only partial discharges.

The frequency of the peaks in the capacitive current show a possible dominant frequency. By calculating the difference between these peaks, different periods were obtained, however the most common period was 554 microseconds, which corresponds to a frequency of about 1,8 kHz.

This frequency has no relation with the input voltage's 50Hz frequency, as we could consider the voltage input as a constant during two separate capacitive current peaks.

Therefore, this frequency must be a function of the medium's dielectric constant, electrode separation and possibly the relative and absolute electrode geometry.

In the following measures this frequency will also be observed.

In this measure, the difference of emitted energy in the capacitive current section and the conduction current section, can be clearly seen. The emitted energy in the latter is greater. This is true for all the following measures.

The lower intensity of the electric field generated by the plate electrode is less efficient in transmitting charge. Nevertheless it produces higher power peaks.

5.3.2.5 15kV

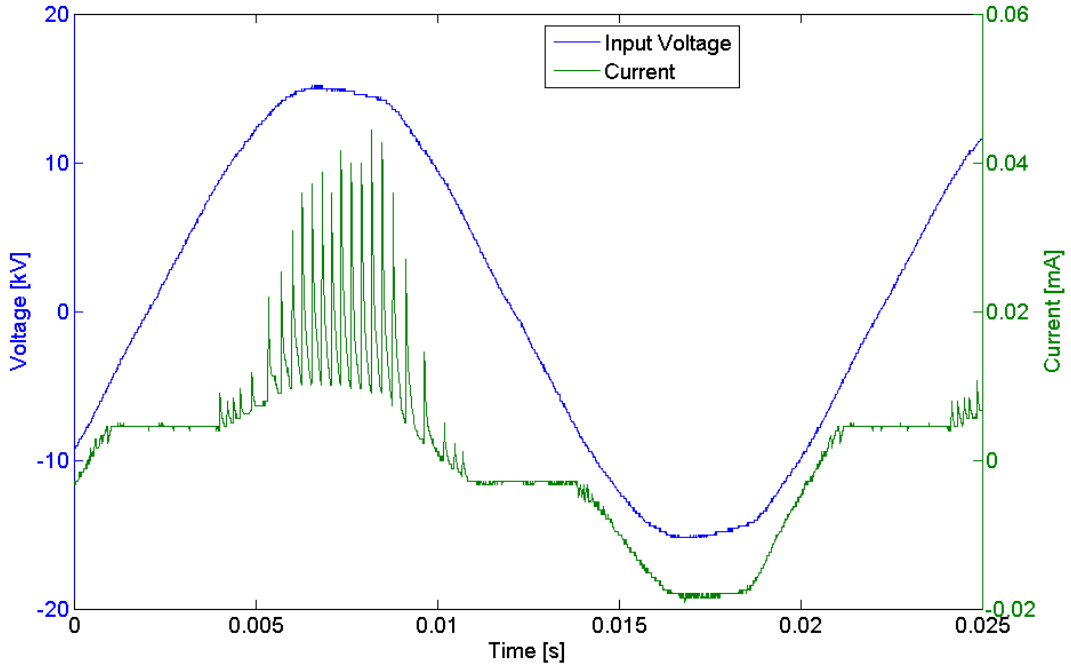

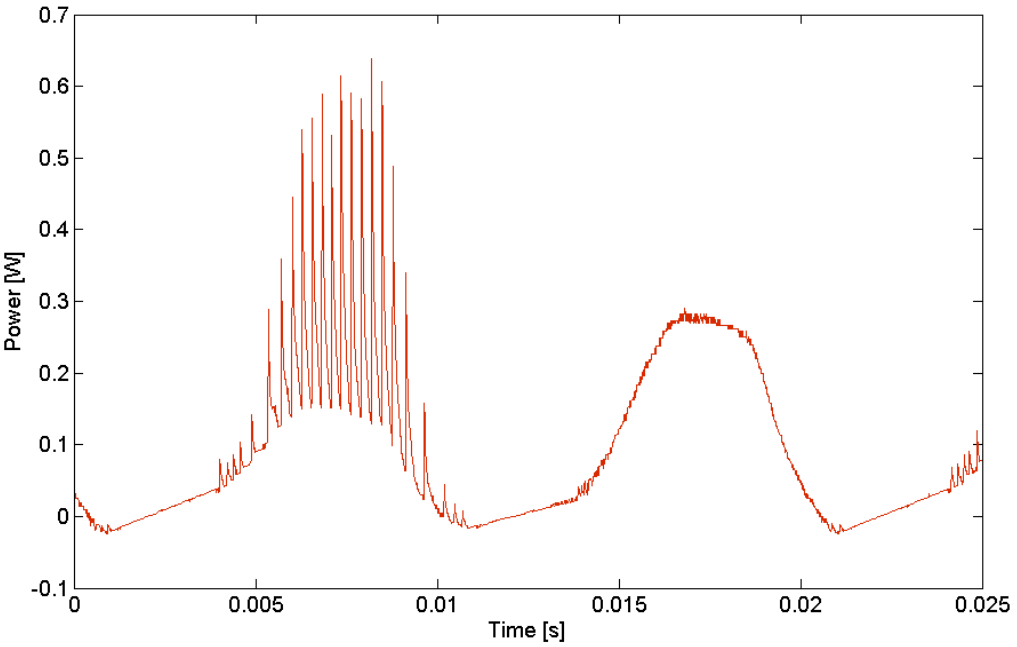

V_{IN}	$I_{conduction}$	$P_{conduction\ max}$	$I_{capacitive}$	$P_{capacitive\ max}$
15kV	~1.966E-5 A	~0.294W	~4.213E-5 A	~0.632W

The frequency of the peaks in the capacitive current show a dominant frequency. By calculating the difference between these peaks, the mean period is 270 microseconds, which corresponds to a frequency of about 3.7 kHz. This is roughly double of the previous measure, which corresponds to the next harmonic.

5.3.2.6 17kV

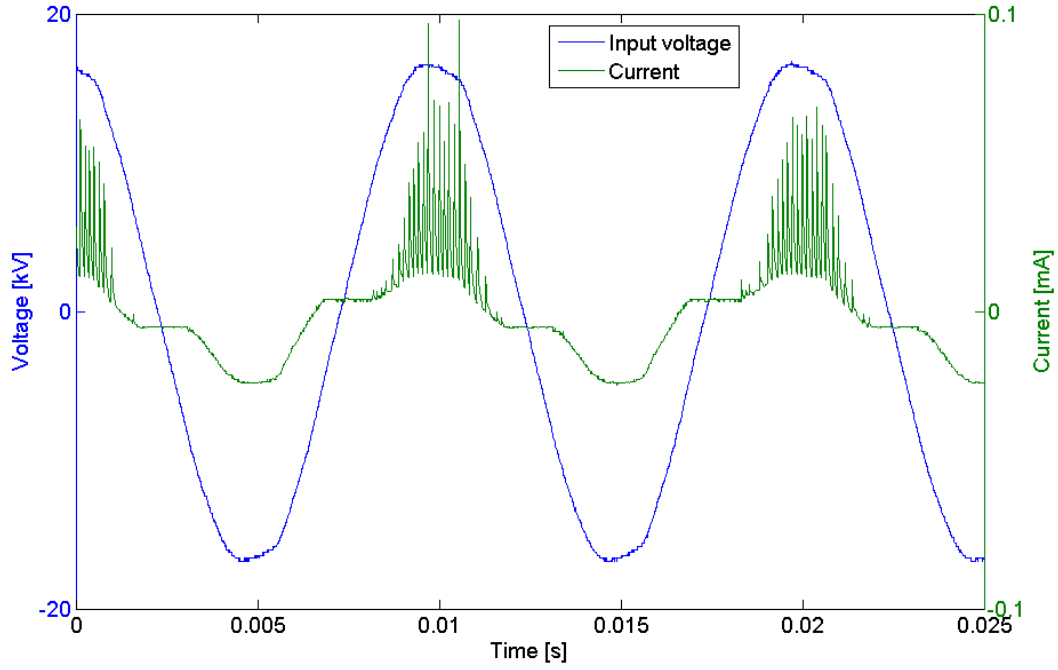

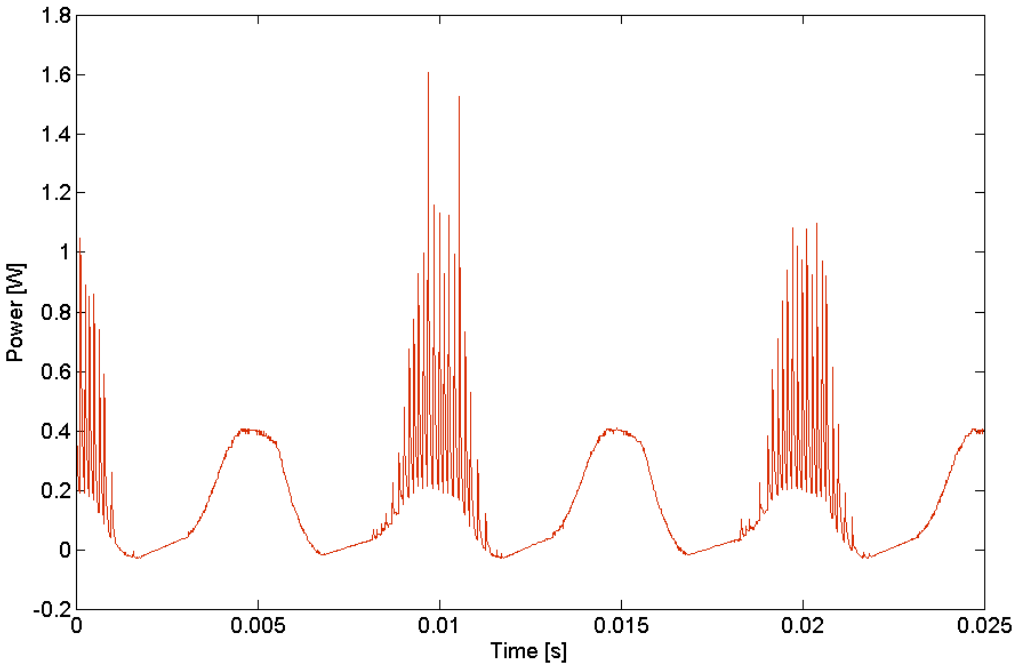

V_{IN}	$I_{conduction}$	$P_{conduction\ max}$	$I_{capacitive}$	$P_{capacitive\ max}$
17kV	~1966E-8A (the same than at 15kV)	~0.334W	~8708E-8 A	~1.48W

During the positive semi-period, the dielectric is partially ionized and produces peaks corresponding to the partial discharges to the medium. During the negative semi-period, the medium is completely ionized and charge is transferred, seen in the oscilloscope as a synchronous voltage variation, which indicates electrical current is circulating through the medium.

At this voltage the frequency has doubled again. With a period of about 121 microseconds, the frequency is set at around 7.6 kHz; the following harmonic.

5.3.3 General analysis

In the preceding graphs, each step in input voltage corresponds to a phenomenon shifting or appearing on the oscilloscope.

It is interesting to note how the current increases from 6 to 12.5 and plateaus between 15 and 17kV input voltage.

This may be due to the fact that the release of electrical potential accumulated in the high gradient areas reaches a value above which the available charge to emit is depleted with each partial capacitive discharge.

Meanwhile, power continues to increase, as it is a function of the increasing input power as well as current.

5.3.4 Alternative construction

The previous setting was dangerous for the oscilloscope, as an arc would produce a voltage drop greater than 300V in the shunt resistor and could potentially destroy the oscilloscope.

To avoid this, a second shunt resistor was built using a large resistor in series between the electrode and the coaxial shunt resistor. This allowed for lower voltage drops in the shunt resistor (less resistance) by bearing the entire voltage drop on the large series resistor.

This caused the total sum of resistances to be high, which was hypothesized to be desirable to avoid arc and increase partial discharge. This hypothesis was derived from the fact that an arc conducts much higher peak currents than partial discharge so, the lower the current, the weaker the arc.

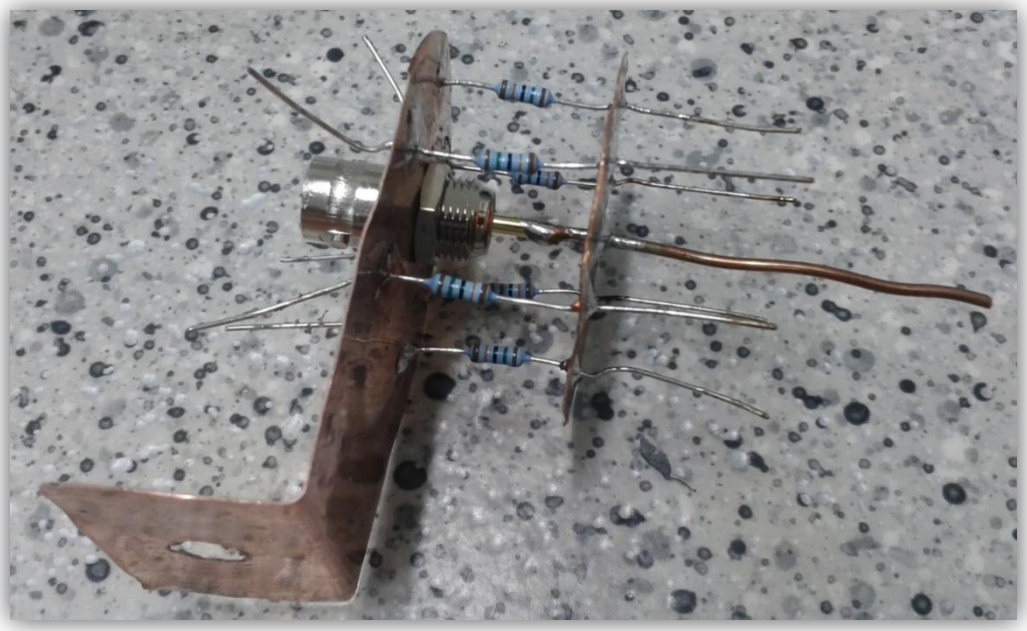

Fig. 36 Image of the shunt-electrode device before it was finished.

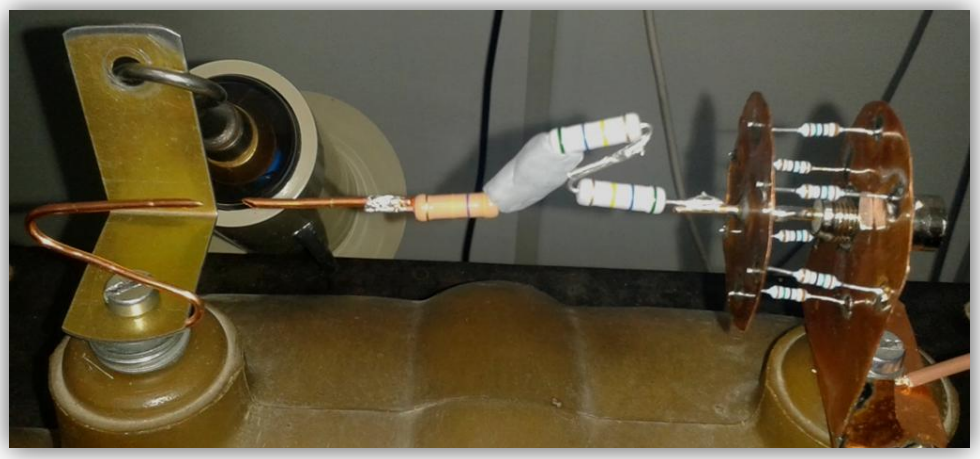

Fig. 37 Image of the finished shunt-electrode device. Note the large series resistors between the high frequency shunt resistor and the tip of the electrode.

This approach proved to dampen the partial discharges by narrowing the interval between no conduction and arc.

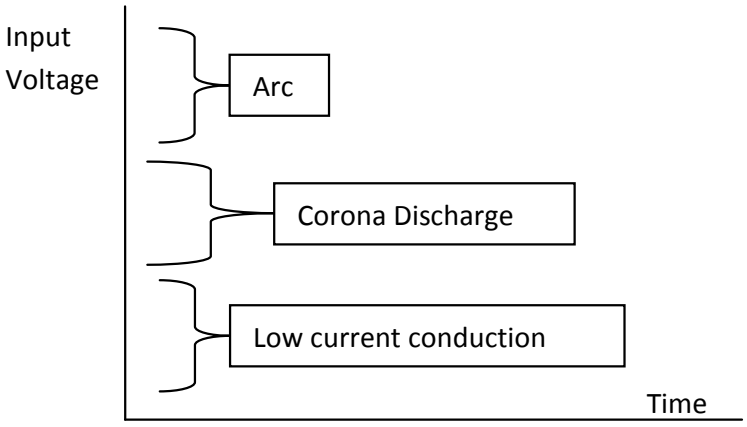

Fig. 38 Qualitative designation of voltage intervals related to the resulting phenomenon.

The resulting experiments failed to produce partial discharges, while still allowing for low current arc to occur.

5.3.5 Diode current limiter

To further protect the oscilloscope, a new approach was taken by using semiconductors.

By using diodes to limit maximum current to the oscilloscope, its destruction could be avoided if an arc occurred.

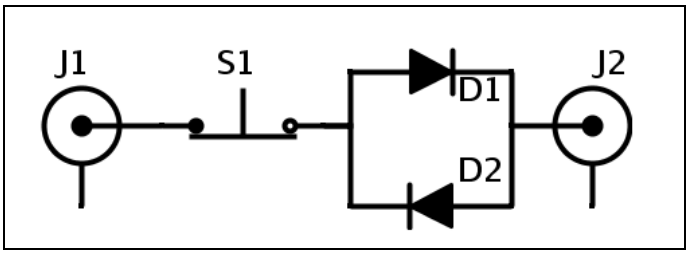

Fig. 39 Circuit diagram of the diode current limiter

The resistors in the shunt were selected to produce a voltage drop no greater than 0.7V. This would allow building a device that would stop a sudden surge to affect the oscilloscope. The device consisted of two anti-parallel diodes. This would limit voltages over 0.7V.

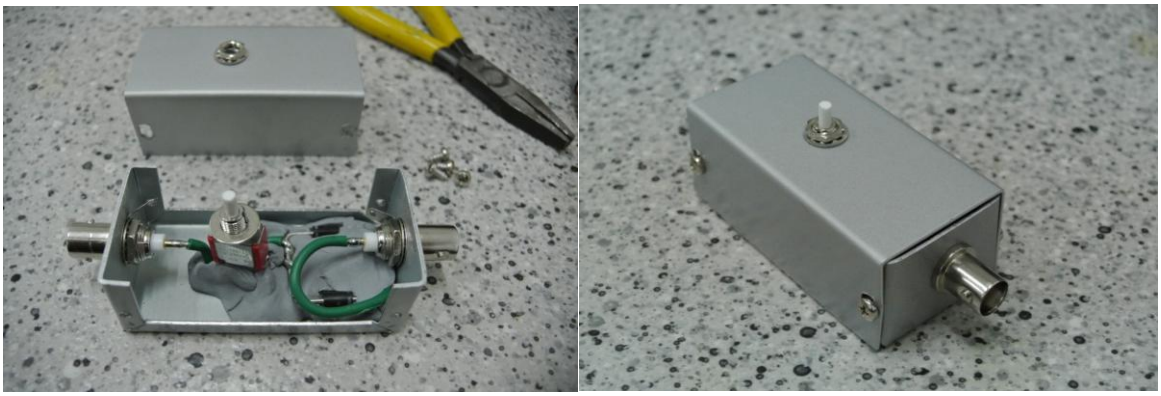

Fig. 40 Image of the metal box in which the circuit was encased (left) and finished device (right).

After producing the setup we designed, it became clear that by limiting the voltage drop to 0.7V, the shunt resistor should have very low resistance.

Tests were made to find the peak voltage in the event of an arc and, in fact, a destructive peak could be avoided only by lowering the shunt resistor voltage to a value for which the current produced a voltage drop under 300V.

Additionally, by eliminating the large resistance hypothesis, disproved in the last shunt, we hypothesized that the corona discharge range would be wider.

5.4 Arc

To compare partial discharge with arc discharge, a third shunt resistor was needed that could probe the conditions of an arc discharge, which are high voltage due to peak currents and very high frequency. The following shunt resistor was designed and built:

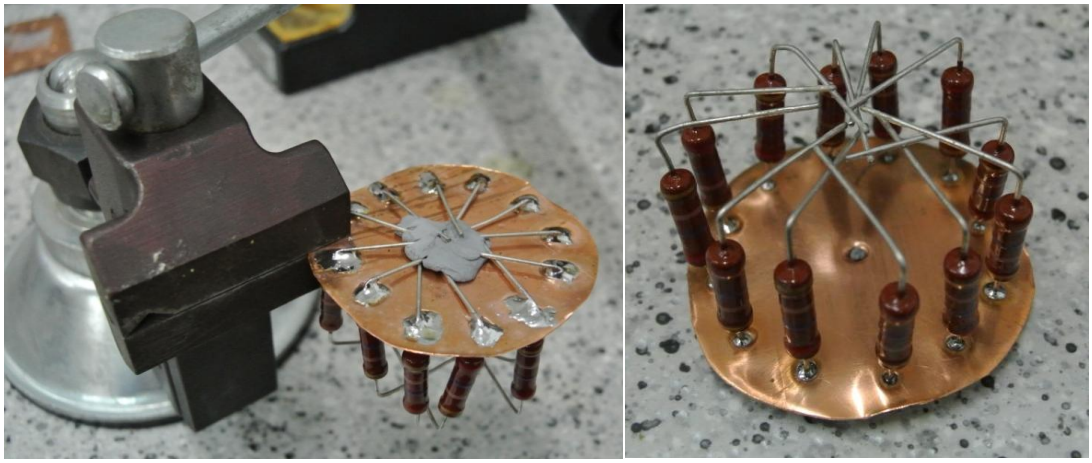

Fig. 41 Images taken during the construction of the high frequency, high current shunt resistor.

Fig. 42 Image of the finished shunt resistor and electrode.

This high frequency shunt resistor consists of twelve 240Ω, 2W carbon resistors. This will allow for a total power dissipation of 24W, while providing low voltage drop (20Ω in theory), in order to protect the oscilloscope input during continuous or peak arc discharges.

The actual resistance was measured at 23Ω.

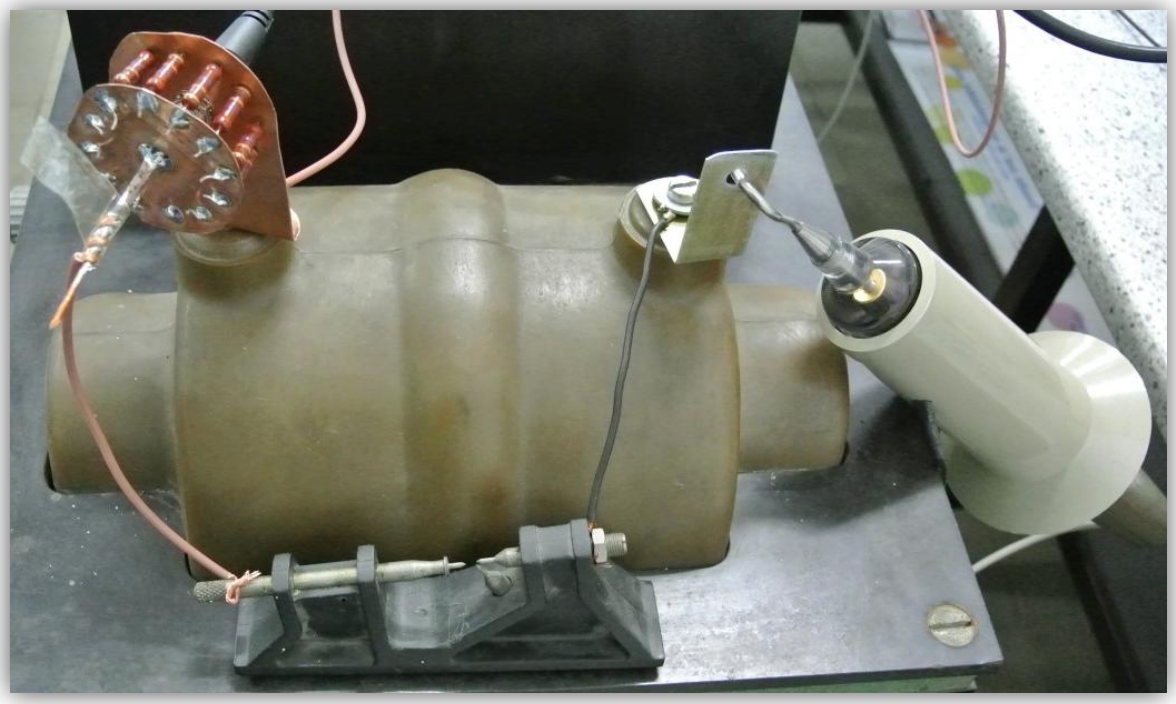

Fig. 43 Image of the high frequency, high current shunt resistor connected to the electrode through a copper wire.

The used electrode tips were especially designed to sustain repeated arc discharges.

For ignition to occur, the transferred energy must be enough for the medium in the space between electrodes to sustain an auto-thermal reaction. That is, that the ignition kernel must develop in spite of thermal losses.

This is accomplished by generating a kernel size several times the width of the flame boundary.

Simultaneously, the size of the kernel must also be such that the radial increase of the reacting volume must be smaller than the burnt volume. That is:

$$\frac{d\left(\frac{4}{3}\cdot\pi((r+\delta)^3-r^3)\right)}{dr} \leq \frac{d\left(\frac{4}{3}\cdot\pi\cdot r^3\right)}{dr} \qquad \text{(Eq. 2)}$$

Where ‘r’ is the volume of the expanding flame boundary sphere. Differentiating, we find the critical radius value:

$$r_c = \delta \cdot \left(1 + \sqrt{2}\right) \cong 2.41 \cdot \delta \rightarrow d_c \cong 5 \cdot \delta \quad \text{(Eq. 3)}$$

Taking into account thermal diffusivity α and the laminar flame boundary speed v_L, δ=α/ v_L, and since $\alpha = \frac{\lambda}{C_p \cdot \rho}$ where λ is the thermal conductivity of the medium, ρ the density and C_p the heat capacity.

$$d_c = \frac{5 \cdot \lambda}{C_p \cdot \rho \cdot v_L} \quad \text{(Eq. 4)}$$

This equation points out the important parameters in arc ignition. The distance between electrodes must be larger than the critical extinguishing distance. With a higher compression, the required distance will decrease, and the leaner the mixture, the larger the distance.

The required energy to ignite this critical volume is as follows:

$$E_{min} = \frac{\pi}{6} \cdot d_c^3 \cdot \rho \cdot \int_{T_0}^{T_a} C_p \cdot dT = \frac{\pi}{6} \cdot d_c^3 \cdot C_p \cdot \Delta T \cdot \rho \quad \text{(Eq. 5)}$$

Experimentally, two models have been found to describe the critical diameter:

$$Low\ turbulence \rightarrow d_c = \frac{10 \cdot \lambda}{C_P \cdot \rho_0 \cdot (v_L - 0.16 \cdot u')} \quad \text{(Eq. 6)}$$

$$High\ turbulence \rightarrow d_c = \frac{10 \cdot \lambda}{C_P \cdot \rho_0 \cdot (v_L - 0.63 \cdot u')} \quad \text{(Eq. 7)}$$

Where u' is a parameter that describes turbulence (Álvarez, Callejón, Carrera, Liesa, Carreras, 1995).

The following experiment will attempt to compare a theoretical ignition by corona discharge with an ignition by arc.

Two arcs were recorded.

5.4.1 Arc #1

First with a gap of 3mm, at 3.4kV (4.4kV amplitude):

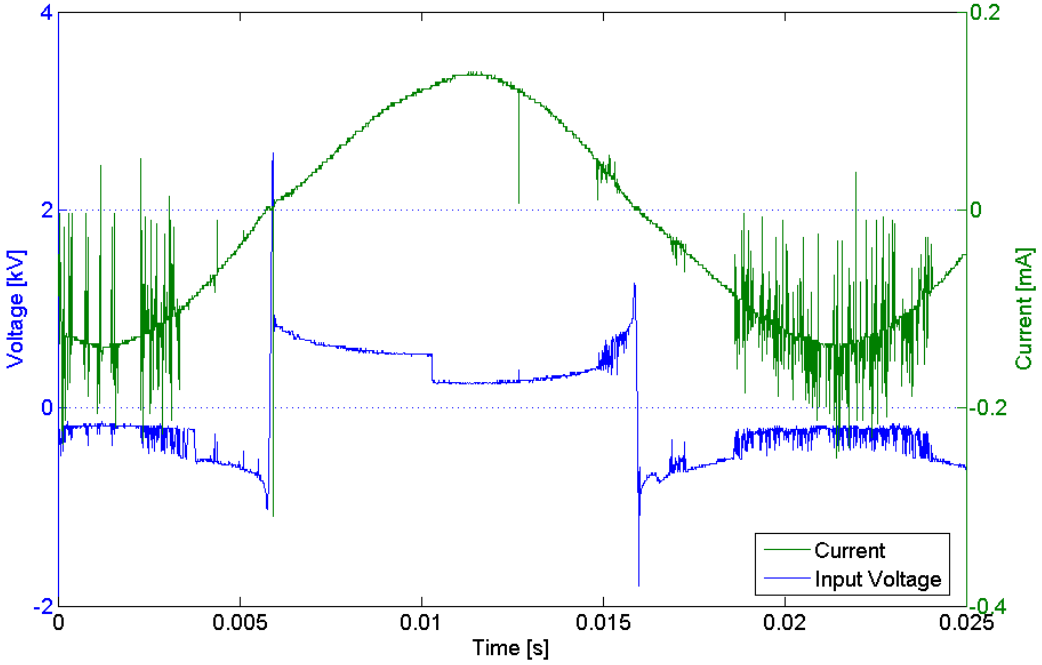

5.4.2 Arc #2

The second with a 6mm gap, at 4.5kV (7kV amplitude):

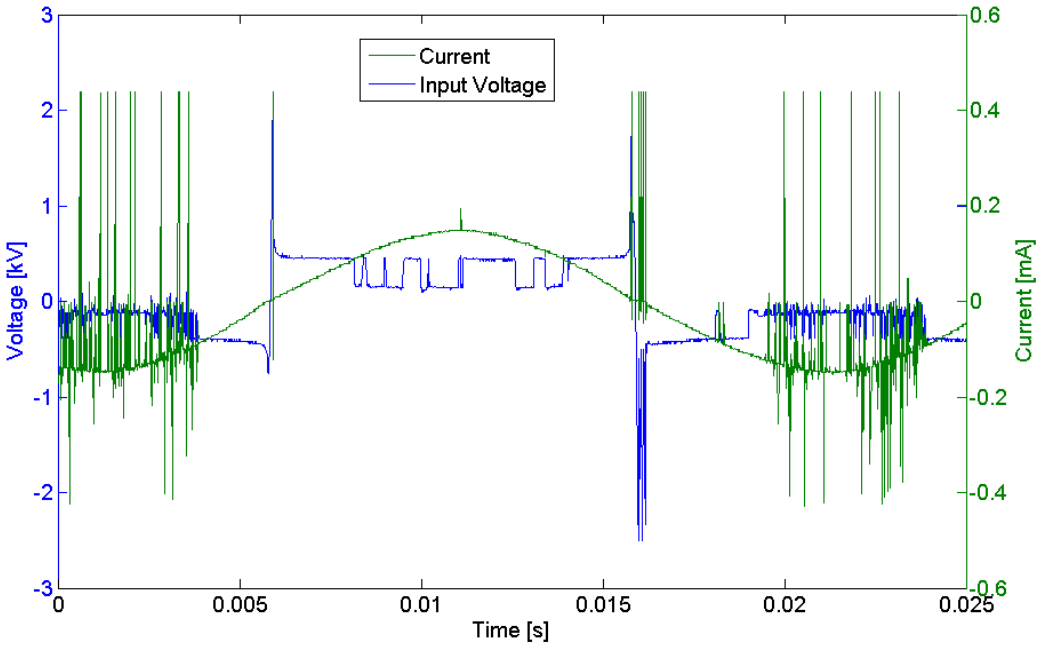

5.4.3 Analysis

It is interesting to note the difference between the partial discharge graphs and the arc discharge graphs.

In the former, the input voltage remains constant while the transferred current peaks. This is because the dielectric barrier is never completely broken, and charge flow is met with high resistance.

However in the latter, the current follows a fairly clean sine wave, as current is transferred between electrodes in a short circuit, while the voltage appears chopped due to dielectric switching between breakdown and recover.

The dielectric rupture happened at higher voltages, proportional to the larger gap, however, interestingly, once the arc is established, both graphs show similar values. This is because an arc acts as a short circuit. The resistance to current flow in the arc is very small due to the high density of free electrons, and thus gap distance has little effect.

It is also interesting to see how the polarity has an effect on the conduction. This is caused by the air, opposing resistance to switching polarities at the 50Hz rate. In negative polarity the air becomes conductive with very low resistance, while in positive polarity the air offers high but unstable resistance to current, due to the higher dielectric being perforated.

By importing the collected data points to Matlab, the transferred energy was calculated as

$$E = \int_{t1}^{t2} (V_{shunt} * \frac{1A}{23V}) * V_1 * 1000 \, dt \qquad \text{(Eq. 8)}$$

The result being **0.318J** of energy released in the negative semi-period of 10ms.

Of course this is a very high amount of energy compared to a sparkplug, because the arc was sustained for 10ms instead of just some microseconds a sparkplug arc typically lasts.

5.5 Point-point partial discharge

To produce a partial discharge the gap was risen to 20mm, while still using the same 23Ω high-frequency shunt resistor.

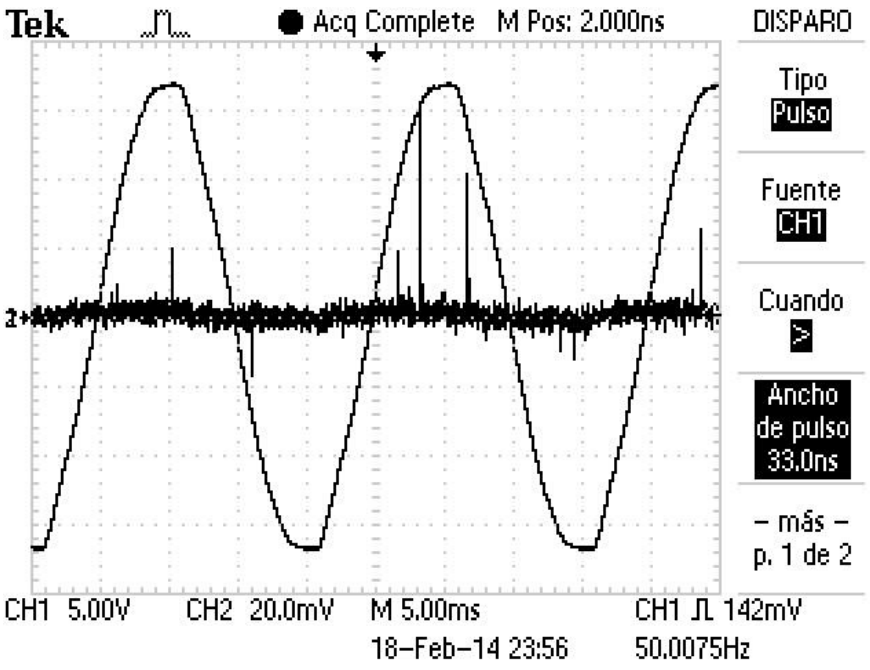

Fig. 44 This image shows the partial discharge display, as a screenshot of the oscilloscope's readings.

Note how the current can be faintly seen oscillating with a 90º delay behind the input voltage, just like during the point-plate experiments with no continuous conduction.

Continuous conduction achieved only by partial discharges could not be achieved with point-point electrodes because the field gradients are higher, thus creating an easier path for a partial discharge streamer to short circuit the dielectric medium and cause a full arc discharge.

Therefore, discharges transition directly from dielectric uphold to dielectric breakdown and arc, without a transitory breakdown/recovery input voltage interval like in point-plate experiments.

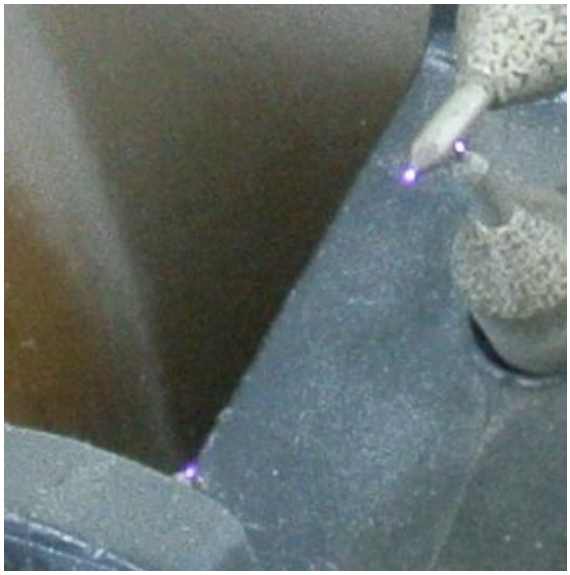

Fig. 45 In this image, the tips of the electrodes can be seen glowing bright purple from the corona discharge photon emissions. This long exposure image was taken with considerably high ambient light, thus the glow is only seen on the very tip, where the electric field gradient is highest.

5.5.1 Partial discharge peak characterization

By setting a trigger for the shunt voltage high enough, several partial discharges were captured:

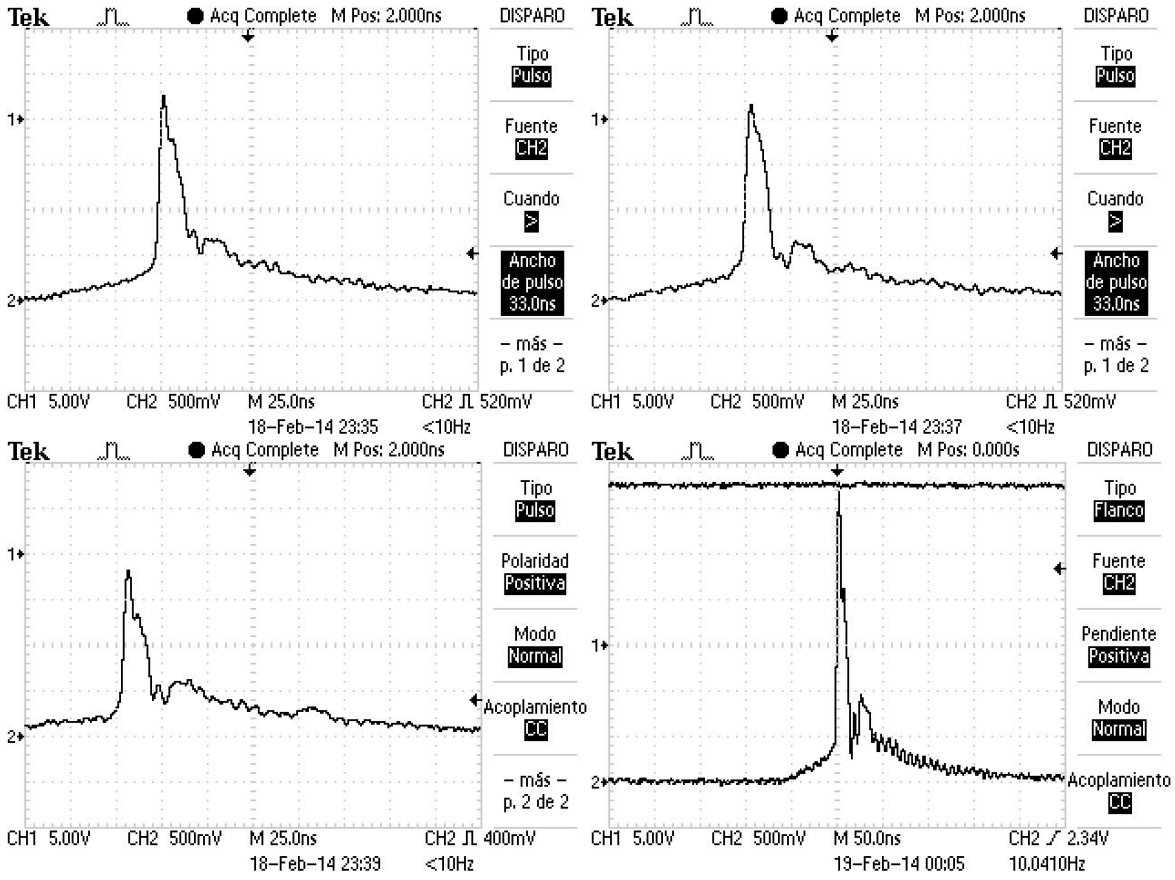

Fig. 46 These are four screenshots of partial discharge peaks taken directly from the oscilloscope. Note how remarkably similar in shape they are. Note also the 25-50 nanosecond time scale. In the bottom right image, the input voltage signal is visible as a constant horizontal line, just on top of the peak.

A qualitative approach was taken to analyze the magnitude of the partial discharge peaks. The trigger threshold was set increasingly high and the time required for one peak of that magnitude to appear was measured.

At 11.4kV RMS, the qualitative results showed that under 1.2V (measured shunt voltage drop) the discharges were continuous. From 1.2 to 2.5V there was some minor delay detected, between 150 and 500 milliseconds. From 2.5V onward, a sample was acquired only every few seconds.

Furthermore, an interest was taken into positioning where the different magnitude discharges occurred in relation to the input voltage sine wave.

To detect this, a time scale was fixed in order to see a full sine wave cycle on the oscilloscope's screen; then, starting from a large trigger value for CH2, the value was consistently decreased. This setting aligned the input voltage sine wave with the oscilloscope's Y axis, depending on where the trigger was fired, shifting the input voltage sine wave, and thus revealing where the partial discharge peaks were happening.

Peak voltage range	**Region of the input voltage sine wave where the corresponding peaks are most common**
>3.5V	Unknown. Too few occurrences to determine with this method
3.5 to 2.5V	Partial discharge peaks are centered in the negative semi-period
.9 to 2.5V	The peaks are biased toward the second quarter of the negative semi-period as the trigger voltage drops. These peaks are very precise and frequent, producing a very clear image on the oscilloscope
.5 to .9V	The partial discharge peaks of this magnitude occur mainly in the transition between negative and positive input voltages
<.5V	Apparently chaotic

5.5.2 Analysis of a partial discharge peak:

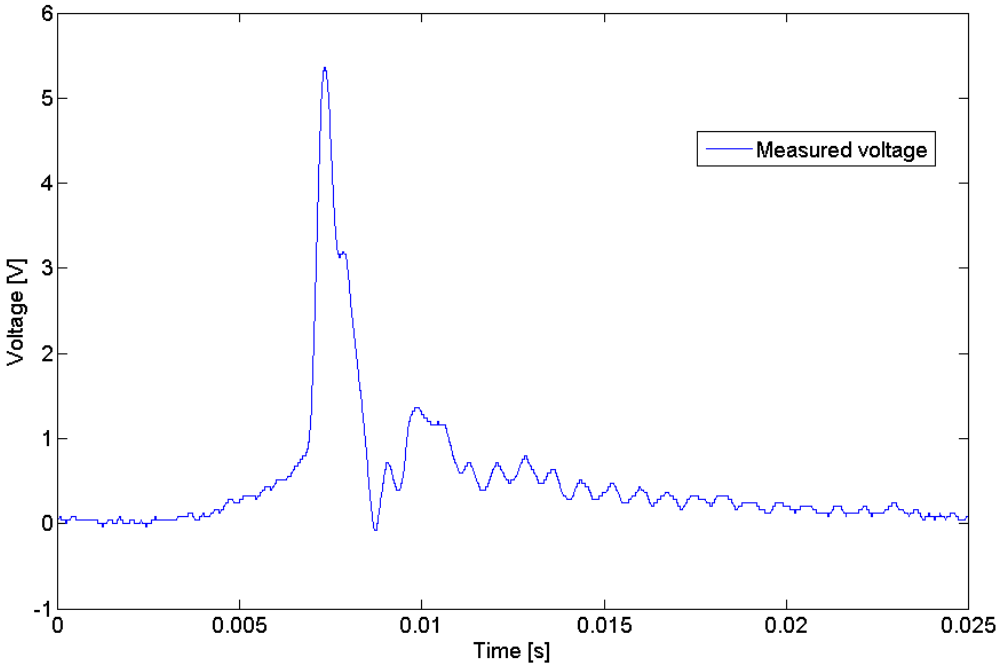

In this partial discharge peak the input voltage is 17.5kV (which can be considered continuous throughout this time frame), the shunt voltage drop is 5.4V, which means a current peak of:

$$I_{peak} = \frac{V_{peak}}{R_{Shunt}} = \frac{5.4V}{23\Omega} = 0.235A = 235mA \qquad \text{(Eq. 9)}$$

To calculate the energy released in the peak, a minimum voltage was selected to limit the beginning and end of the peak. This threshold voltage was set at 0.4V.

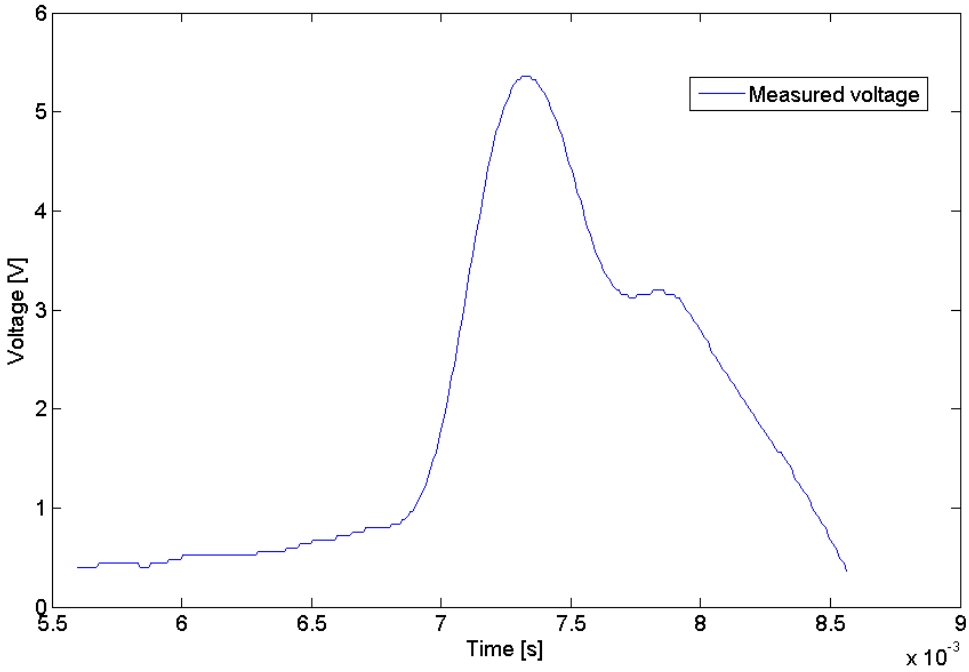

By integrating the power along time, the energy released in this one peak was 4.2291e-5J or .0423mJ. The total energy released, setting 0V as the threshold, was 9.2485e-005 or .0925mJ. The peak power is strikingly high, at 3.8kW.

In theory, these energy values are too low to produce ignition. However, even though this particular peak is very high, lesser peaks occur in rapid succession, even though the alternating input voltage oscillates at only 50Hz.

Since different magnitude peaks occur in specific regions of the sine wave, it would be interesting to increase the high energy peak density by increasing the input voltage frequency.

This magnitude is significantly higher than the measurements taken with point-plate electrodes.

A possible explanation for these measurements is that because the field gradient occurring in pointed electrodes is greater, the medium opposes less resistance to polarization upon partial discharge.

It may as well be the case that as both electrodes have a very high charge density, when a partial discharge occurs, the flow of charges required to release the potential between electrodes is higher, resulting in increased measured currents.

In any case, the objective is to transfer energy into the medium and not to the opposite electrode; therefore, a means to measure energy release into the medium should be devised in future studies.

5.6 Ignition tests

5.6.1 Methodology

The working hypothesis is that in a partial discharge the affected volume is between two and three orders of magnitude greater than in an arc discharge.

A paper tube, and later also a transparent acetate plastic tube, was attached to the outlet of a blowtorch. This avoided coming into close proximity of the high voltage electrodes and risk severe electrical shock. The paper heated up significantly but did not ignite, while the acetate plastic melted, so it had to be changed every few ignition tests. The advantage of plastic is that its transparency allowed for a better visual impression of the phenomenon.

Three scenarios were observed:

1. The corona discharge successfully ionizes the air-propane mixture creating a chain reaction which causes ignition.
2. The change in composition and flux brought on by the mixture lowers the medium's resistivity and an arc occurs, igniting the mixture.
3. The mixture is unaffected by the ongoing corona discharge.

The working hypothesis was that the corona discharge would trigger the ignition. During combustion, due to the ionization of the flame boundary, the partial discharges would become an arc and the transformer's power breaker would trigger.

Several tests were conducted by igniting a stream of propane-air mixture. These tests were recorded by a high speed camera, recording at 1200fps, to determine the cause of ignition.

5.6.2 Results

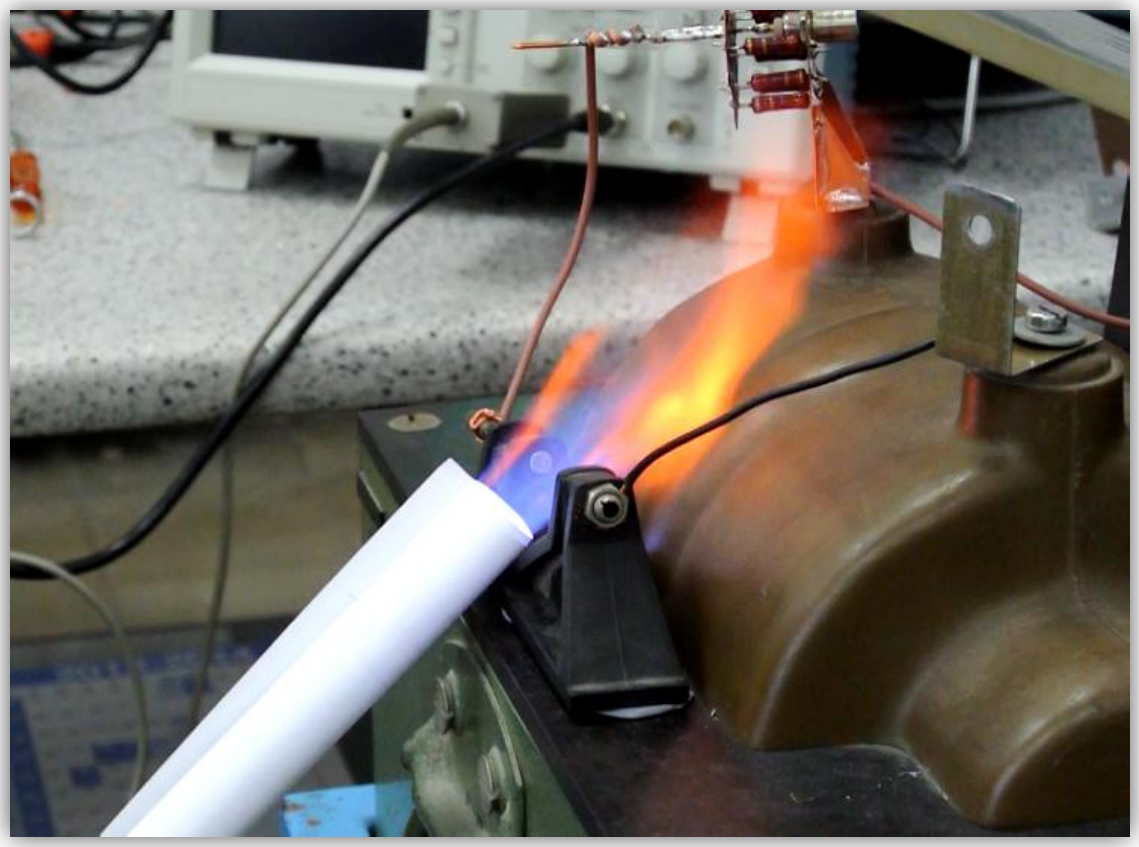

Fig. 47 Ignition of the propane-air mixture.

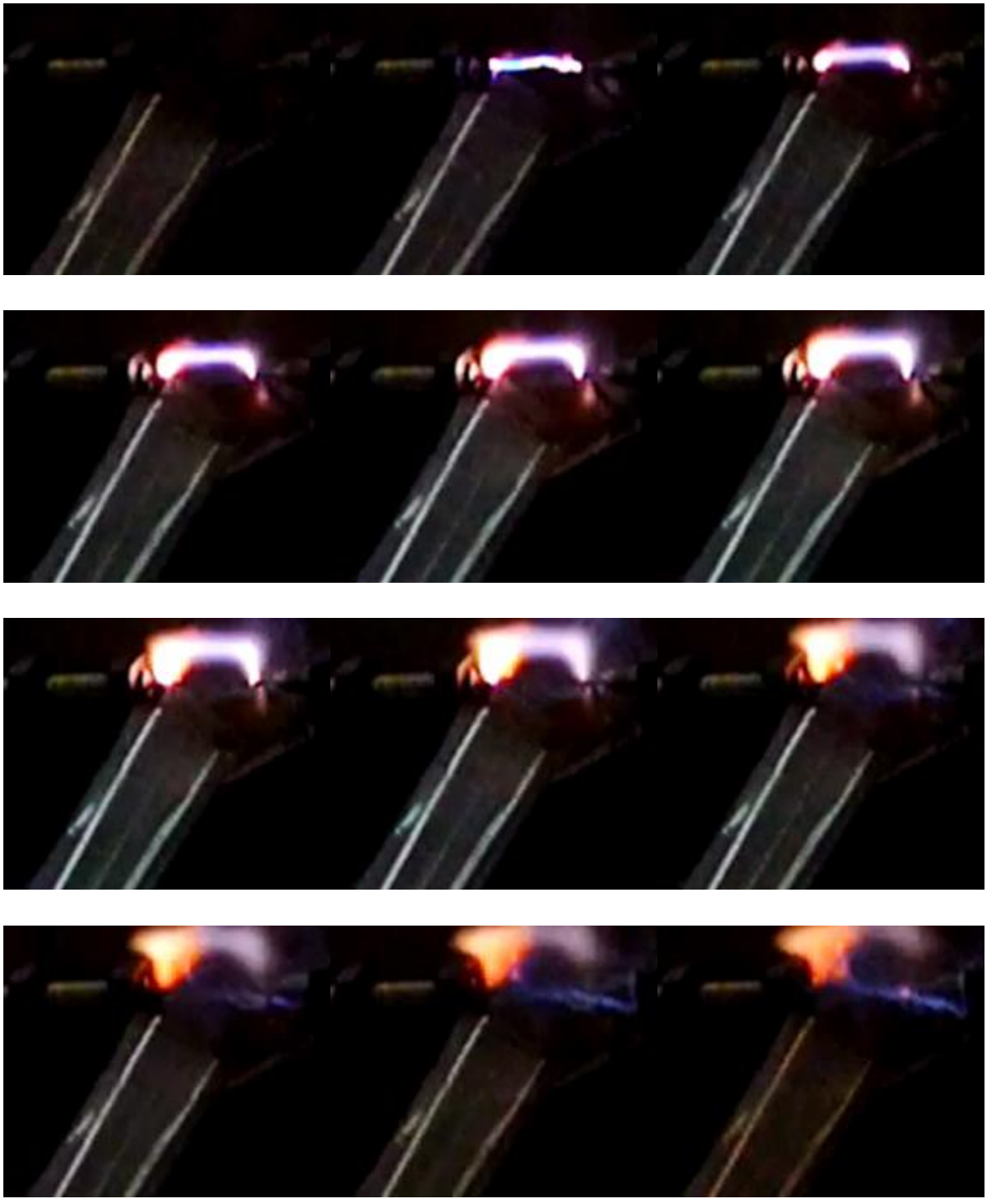

Fig. 48 These images correspond to the high speed video, frame by frame. Each frame is 0.8 milliseconds apart, so the whole 12 frame sequence happens in 10 milliseconds, that is, half a 50Hz wavelength.

It is interesting to note the distinct coloration on the anode and cathode, typical of arcs.

What the high speed camera captured was that the arc triggered the combustion and not the other way around, as hypothesized.

To verify this result, the same was attempted with a point-plate setting. Ignition was not achieved, as the arc was not triggered. Although the partial discharge in point-plate electrodes had much lower transferred power readings.

Interestingly enough, after these results, air was blown in the attempt to rule out the speed of the fluid being the trigger of the arc. The arc was indeed triggered by blowing air onto the gap in a point-plate setting.

This was done using a long paper tube and air was blown using our lung power.

The composition of breath is very similar to the composition of air; however it contains:

- Significantly more water (humidity) and
- It's hotter

These two factors may be enough to trigger an arc discharge, as both directly lower the conductivity of air.

Nevertheless, it is reasonable to think that the air flow and turbulence is also a determining factor in measuring the resistance to ionization of a medium. This is a matter for future study.

The point-point electrode setting is not able to transfer enough power to the mixture through corona discharge, even though the electric energy measures were very high.

These results don't agree with the scientific background that inspired the setting. A new study is required that takes into account other parameters, such as high frequency.

6 Budget

As this project consists of a preliminary study, the financial details include only the purchased materials, used instrumentation and support, and labor.

There is no expected return of investment, as no technological solution has been determined yet.

The amortization of instruments and support has been taken into account as a partial amount of the used unit.

Category		Goods and services	Price	Units	Total price
Labor		Engineering/design	70.00 €	200	14,000.00 €
		Experimenting	50.00 €	150	7,500.00 €
		Reporting	20.00 €	150	3,000.00 €
	Subtotal				24,500.00 €
Instruments and support		Asus © PC	500.00 €	0.1	50.00 €
		Matlab © R2009b 32bit software	2,000.00 €	1	2,000.00 €
		Microsoft Office ©2010 software	120.00 €	0.15	18.00 €
		Tektronix © Oscilloscope	1,200 €	0.9	1,080.00 €
		Nikon © 1 J2 camera	600 €	1	600.00 €
	Subtotal				3,748.00 €
Materials		Electronic parts	-	-	-
		Copper foil	-	-	-
		Solder	-	-	-
		Copper cables	-	-	-
	Subtotal				50 €
	Total				**28,298.00 €**

Conclusions

The use of corona discharge phenomenon as an improved ignition device presents many promising advantages:

- It can deliver high power into the medium
- It can deliver high energy into the medium
- It affects a volume far greater than in other ignition technologies, reducing the restraints of flame boundary speed
- It provides further lines of investigation on lowered emissions both by burning less fuel and by altering emissions' electro-chemical properties

The reduction of pollutants, increase in burn performance, efficiency and increase in versatility for highly demanding applications are all very interesting features, fit for a new generation of internal combustion engines.

However, there are still many details which are yet to be properly studied. The measurements obtained from the experiments are very encouraging from a physical phenomenon point of view but are yet to be successfully studied, implemented and refined for engineering applications.

These partial results will provide leads for other research projects, briefly described in the following 'Future work' section.

The point-plate study was particularly interesting, as key parameters that determine the corona discharge phenomenon were recorded. Two distinct means for transferring charge from one electrode to the other were observed, named conduction and capacitive current.

These two current wave shapes, reflect how the electric field generated by two differently shaped electrodes are dramatically different, and have an impact on the transferred power and energy during partial discharges.

Current varies nonlinearly with voltage increase. The increase in voltage has a secondary effect: it creates a stronger electrical field which modifies the dielectric properties of the medium. By changing the composition of the medium (e.g. by adding hydrocarbon gas for ignition) the dielectric properties change with it.

The frequency of the capacitive current doubled its frequency from 12.5 to 15 kV and from 15 to 17 kV. It would be interesting to find what phenomenon dominates at higher frequencies, and if an optimal frequency and amplitude can be found to optimize energy transfer into the medium.

However the power transfer between electrodes was lower than using point-point electrodes.

These high frequency, low intensity discharges should be further studied as it may be possible that this effect is not desired in corona discharge devices because of the phenomenon's similarity to an arc.

The only difference from an arc would be that the medium has enough ionizing capacity to oppositely polarize the incipient arc before it produces a plasma stream reaching the opposite electrode.

This is undesired as the affected volume is very low, as well as the energy compared to an arc.

Future work

For future studies, here is a list of leads I believe would be interesting to further investigate, following this study's results:

- To measure the current throughput of both electrodes to validate charge transmission from one to the other or, by the contrary, measure current released into the medium. This would allow to quantify the ionization of the medium and to verify the effect on the medium of a corona discharge.

- To increase the frequency up to several kHz. The next step in this project's setting was to build a high frequency, high voltage generator using a fly back transformer (for example, one found in a CRT monitor). The input would be generated in an oscillator, and then amplified to some tens of kV. The combination of high voltage with variable frequency would provide information on the best combination for optimal medium ionization and high energy emission.

- To plot the voltage range at which ionizing conduction, corona discharge and arc happen, depending on frequency.

- The effect of medium composition, flow and turbulence in corona discharges.

Acknowledgements

This study has had two direct and many indirect collaborators.

First of all I'd like to thank my tutor, Dr. Jesús A. Álvarez Flórez, who has given me invaluable guidance and support. I have found his interest in the project contagious and very inspiring.

I'd like to thank Dr. Ricard Bosch Tous as well, for the interest he took in the study and the support in my understanding of some key issues in high voltage engineering problems.

Many thanks as well to all the indirect collaborators.

References

About.com, I. (n.d.). *The History of the Automobile*. Retrieved 10 2013, from http://inventors.about.com/library/weekly/aacarsgasa.htm?rd=1

Álvarez, Callejón, Carrera, Liesa, Carreras. (1995). *Fenomenología del encendido en motores de ciclo Otto.* Barcelona: CPDA ETSEIB-UPC.

Babrauskak. (2003). Ignition Handbook. Issaquah, WA: Fire Science Publishers.

Beggs. (2006, October 24). What is a corona discharge and how does it work? Medical Biophysics Group, University of Bradford.

Bellenoue, L. E. (2005). Corona discharge ignition and combustion promotion of methane/air mixtures. *Proceedings of the European Combustion Meeting* , 6.

Commission Regulation (EU) No 582/2011. (2011, May). *http://eur-lex.europa.eu/.* Retrieved April 2014, from Access to European Union Law: http://eur-lex.europa.eu/LexUriServ/LexUriServ.do?uri=OJ:L:2011:167:0001:0168:EN:PDF

Dale, Checkel, Smy. (1997). Application of high energy ignition systems to engines. *Prog. Energy Combust. Sci. Vol. 3.* , 379-398.

Hargreaves. (2013). Maik Merke. Federal Mogul's programme manager for ignition products. *Automotive Engineer* , 15.

MIT - Unified Engineering, S. (n.d.). *11.6 Performance of Jet Engines*. Retrieved from http://web.mit.edu/16.unified/www/SPRING/propulsion/notes/node85.html#SECTION06363300000000000000

Ronney. (2004, 10). *Corona Discharge Ignition.* Retrieved 8 2013, from http://carambola.usc.edu/research/coronaignition/coronaengine.html

van Veldhuizen, Rutgers. (2001). Corona discharges: fundamentals and diagnostics. *Proceedings of Frontiers in Low Temperature Plasma Diagnostics, Limburg IV* .

Vinogradov, Rivin, Sher. (2006). NOx reduction from compression ignition engines with pulsed corona discharge. *Elsevier* .